Serial No. 471,461

Filing Date 6 June 1995

Inventor Robert W. McElhanon
William K. Burns

NOTICE

The above identified patent application is available for licensing. Requests for information should be addressed to:

OFFICE OF NAVAL RESEARCH
DEPARTMENT OF THE NAVY
CODE OOCC3
ARLINGTON VA 22217-5660

FIBER OPTIC DIGITAL TRANSMISSION SYSTEM

Cross Reference to Related Patents and Applications

This application is a Continuation in Part of commonly assigned and co-pending U.S. Application Serial No. 08/258,028 filed June 10, 1994 by the inventors Ganesh K. Gopalakrishnan and William K. Burns and having docket no. NC 75,680 and is entitled to the benefit of the June 10, 1994 filing date for the matter disclosed therein. U.S. Application Serial No. 08/258,028 is incorporated herein by reference.

Background of the Invention

The present invention relates to fiber optic links for signal transmission, and more particularly, to microwave subcarrier multiplexed systems.

Description of the Related Art

A mixer is a nonlinear device which combines signals of different frequencies to produce a common output signal having the sum or difference. Typically, a local oscillator (LO) reference signal is applied to one of the mixer ports, and a weaker signal (RF) to be converted is applied to a second mixer port. Sum or difference (IF) frequencies of the input signals and, usually, other higher order harmonics appear at the output port of the mixer. For transmitter application, an information

bearing signal is upconverted through a mixer to a higher RF microwave frequency and is usually amplified before being transmitted. This up-conversion usually involves the sum frequency. For receiver application, a received microwave signal is down-converted through a mixer to a lower IF frequency, which is then demodulated.

In conventional optoelectronic receivers, RF signals transmitted over an optical fiber are detected with a photoreceiver, following which down-conversion to an IF signal is accomplished through a conventional microwave mixer. However, there are several difficulties associated with this approach. If the transmitted optical signal is modulated at millimeter wave frequencies (the carrier frequency), then a high-speed photoreceiver is necessary to detect the transmitted signal. The photoreceiver must have high enough bandwidth to detect the carrier signal. High-speed receivers, because of their fine geometries, typically saturate at fairly low optical power levels. These low power levels may be insufficient to overcome the inherent noise level of the optoelectronic system. Conventional microwave mixers have a limited bandwidth and are limited in port-to-port isolation. Such mixers also have high intermodulation (IM) distortion. Some of these problems can be circumvented by optical down-conversion, thereby eliminating the need for high-speed detection and the microwave mixer.

U.S. Patent No. 5,199,086 to Johnson proposes an electro-optic mixer system using two electro-optic interferometric waveguide modulators coupled in series. However, the electro-optic modulators in the Johnson system may have high drive voltage. As a result, the mixer system proposed in Johnson would have high insertion, i.e. conversion loss and thus low efficiency. Such a system is not practical because, as with the conventional optoelectronic receivers, the modulation effect in the modulated optical signal would be masked by noise.

Transmission of digital signals over an optical fiber offers the advantage of low-loss and lack of electromagnetic interference, and several approaches for fiber optic links have been proposed. However, one such approach, resonant enhancement of semiconductor lasers, provides a system of narrow bandwidth, and another such approach, phase-locked distributed-feedback laser systems, has limited bit transmission rates.

Summary Of The Invention

It is an object of this invention to provide a fiber optic link for data transmission using microwave subcarrier multiplexing.

It is a further object of this invention to provide a fiber optic link for digital data transmission using microwave subcarrier multiplexing.

It is another object of the invention to provide a fiber optic link for digital data transmission using subcarrier multiplexing that can concurrently detect and down-convert microwave signals using low-speed photoreceivers.

Another object of the invention is to provide a fiber optic link for digital data transmission using subcarrier multiplexing and external modulation.

These and other objectives are achieved by a transmission system responsive to an electrical input information signal which includes means for modulating the input signal with a microwave subcarrier signal to produce a subcarrier modulated signal. A first interferometric modulator responsive to a source light and to the subcarrier modulated signal produces a first modulated optical signal. A second interferometric modulator cascade coupled to the first modulator and being responsive to the first modulated optical signal and to a microwave local oscillator signal produces a second modulated optical signal. Means coupled between the first and second modulators transmit the first modulated optical signal from the first modulator to the second modulator. Means responsive to the second modulated optical signal produce an output signal.

These and other objects, features and advantages of the present invention are described in or apparent from the following detailed description of preferred embodiments.

Brief Description Of The Drawings

The preferred embodiments will be described with reference to the drawings, in which like elements have been denoted throughout by like reference numerals, and wherein:

Figure 1 shows in block diagram form an electro-optic mixer of the present invention.

Figure 2A illustrates a coplanar strip (CPS) electrode structure.

Figure 2B illustrates a coplanar waveguide (CPW) electrode structure.

Figure 3 illustrates dispersion curves for substrate modes of Z-cut lithium niobate ($LiNbO_3$) slabs or substrates.

Figure 3A illustrates an exemplary Z-cut $LiNbO_3$ substrate from which was derived the waveform for the TM_0(cond) substrate mode shown in Figure 3.

Figure 3B illustrates an exemplary X- or Y-cut $LiNbO_3$ substrate.

Figure 4A and 4B show electrical transmission (S_{21}) plotted against frequency for different substrate thicknesses of CPS devices.

Figure 4C and 4D show electrical transmission (S_{21}) plotted against frequency for different substrate thicknesses of CPW devices.

Figure 5 illustrates a cross section of a phase modulator with coplanar waveguide electrodes.

Figure 6 illustrates a top view of the phase modulator of Figure 5.

Figure 7 illustrates a cross section of an intensity modulator with coplanar waveguide electrodes on a Mach-Zehnder interferometer.

Figure 8 illustrates a top view of the intensity modulator of Figure 7.

Figure 9 illustrates a plot of the microwave index n_m against electrode thickness, and a comparison of theoretical results with experimental results.

Figure 10A illustrates the electrical transmission through coplanar microwave waveguides.

Figure 10B illustrates the normalized optical response of the device of Figure 5 or Figure 7 in decibels (dB) of electrical power as a function of frequency.

Figure 11 shows in block diagram form an embodiment of the electro-optic mixer of Figure 1 used in the examples herein.

Figure 12 illustrates the optical response and the RF half-wave voltage for modulators M_1 and M_2 of Figures 1 and 11.

Figure 13 shows the power spectrum of the mixer of Figure 11 for off-quadrature bias.

Figure 14 shows the power spectrum of the mixer of Figure 11 for bias at quadrature.

Figure 15 shows the variation of detected IF power with respect to input RF power for the mixer of Figure 11 when RF=15.52 GigaHertz (GHz) and LO=15.56GHz.

Figure 16 shows the variation of detected IF power with respect to input RF power for the mixer of Figure 11 when RF=40.02GHz and LO=40.06GHz.

Figure 17 shows the variation of detected IF power with respect to input RF power for the mixer of Figure 11 for equal strength RF and LO signals.

Figure 18 illustrates the relation between RF Half-Wave Voltage and conversion loss.

Figure 19 illustrates a mixer employing an erbium doped fiber amplifier between the first and second modulators.

Figure 20 illustrates a mixer employing an erbium doped fiber amplifier to amplify the output optical IF signal.

Figure 21 shows a fiber optic transmission system of the present invention.

Figure 22 shows the error rate of the device of Figure 21.

Figure 23 shows a fiber optic transmission system using multiple subchannels.

Figure 24 shows a fiber optic transmission system including three optical modulators.

Figure 25 shows a fiber optic transmission system using multiple subchannels.

Detailed Description Of The Preferred Embodiments

Referring now to the drawings, Figures 1 and 11 show an electro-optic mixer 10. The mixer 10 includes means 20 for producing first and second microwave signals S_1 and S_2 having first and second frequencies f_1 and f_2, respectively. In other words, the first and second microwave signals S_1 and S_2 have first and second angular frequencies ω_1 and ω_2, respectively. A device 30 provides source light L_i. The device 30 preferably includes a cw laser 32, polarizing optics 34, and a polarization-preserving optical fiber 36 for producing, preferably, polarized light L_i, and most preferably, polarized cw laser light L_i.

The mixer 10 also includes first and second broadband, low drive voltage, traveling wave intensity modulators M_1 and M_2, respectively, which are described further below. The first modulator M_1 is responsive to the source light L_i and to the first microwave signal S_1 for producing a first modulated optical signal L_{m1}. The mixer 10 further includes means 40 coupled between the first and second modulators M_1 and M_2, respectively for transmitting the first modulated signal L_{m1} from the first modulator M_1 to the second modulator M_2. Since the modulators M_1 and M_2 are electrically decoupled, the isolation between their

signal ports is almost infinite, making them attractive for microwave mixing. The transmitting means 40 is preferably, but not necessarily, polarization-maintaining means 40, such as polarization-maintaining optical fiber 40. The second modulator M_2 is cascade coupled to the first modulator M_1 and responsive to the first modulated signal L_{m1} and to the second microwave signal S_2 for producing a second modulated optical signal L_{m2} having a frequency component at the difference $|f_1-f_2|$ between the first and second frequencies f_1 and f_2, respectively. Such an embodiment of the mixer 10 would be useful for down-conversion. Alternatively, the second modulator M_2 is cascade coupled to the first modulator M_2 and responsive to the first modulated signal L_{m1} and to the second microwave signal S_2 for producing a second modulated optical signal L_{m2} having a frequency component at the sum f_1+f_2 of the first and second frequencies f_1 and f_2, respectively. Such an embodiment of the mixer 10 would be useful for up-conversion.

EXEMPLARY MODULATORS M_1 AND M_2

Referring now to Figures 2A and 2B, Figure 2A illustrates an exemplary coplanar strip (CPS) electrode structure in an exemplary Mach Zehnder interferometer modulator, while Figure 2B illustrates an exemplary coplanar waveguide (CPW) electrode structure in an exemplary Mach Zehnder interferometer modulator.

Physically the CPS electrode structure of Figure 2A has a hot electrode 112, to which a modulating signal is applied (not shown), and a single ground plane or grounded electrode 114 on one side of the hot electrode 112. On the other hand, the CPW electrode structure of Figure 2B has a hot central electrode 112A, to which a modulating signal, typically a microwave signal such as S_1 or S_2 (not shown) is applied, and two ground planes or grounded electrodes 114A and 114B on opposite sides of the hot central electrode 112A. The major physical difference between the CPS and CPW electrode structures is that the CPS electrode structure of Figure 2A lacks a second ground plane or grounded electrode. This physical difference results in a crucial operational difference between the use of the coplanar strip (CPS) electrode structure of Figure 2A and the use of the coplanar waveguide (CPW) electrode structure of Figure 2B in an integrated optic modulator. The advantage of the CPW structure of Figure 2B over the CPS structure of Figure 2A will be explained by now referring to Figure 3 and Figure 4A through 4D.

Figure 3 illustrates dispersion curves for substrate modes of Z-cut lithium niobate ($LiNbO_3$) slab (shown in inserts 118A and 118B), which $LiNbO_3$ slab represents a dielectric substrate 116, and where air (having an index = 1) is the material under the $LiNbO_3$ substrate 116. Two different conditions are shown in Figure 3. One condition is with a metal coating 120 on the upper

surface of the dielectric substrate 116, while the other condition is without the metal coating 120 on the upper surface of the dielectric substrate 116. The effective index n_m of the guided modes of the Z-cut $LiNbO_3$ slab is plotted against the ratio of h/λ_0, where h is the substrate 116 thickness and λ_0 is the free space wavelength.

Shown in Figure 3 are five substrate modes, respectively labeled TE_0(die), TM_0(cond), TE_1(cond), TM_0(die) and TE_1(die), where:

TE_0 (transverse electric) means that the electric field is parallel to the plane of the slab (and the magnetic field is perpendicular to the plane of the slab),

TM_0(cond) represents the TM_0(cond) substrate mode for a Z-cut $LiNbO_3$ substrate 116,

TE_1(cond) represents the TE_1(cond) substrate mode for a Z-cut $LiNbO_3$ substrate 116.

the subscripts 0 and 1 refer to the order of the substrate mode, with 0 and 1 respectively representing the first order mode and the second order mode,

(die) represents an approximation of the CPS structure based on the assumption that substantially no metal is disposed on the top of the dielectric substrate 116,

(cond) represents the CPW structure where metal 120 (a conductor) is disposed on the top of the dielectric substrate 116,

2.15 = the optical index in $LiNbO_3$ at a wavelength of 1.3 micrometer (μm),

h = the thickness of the substrate 116,

λ_0 = free space microwave wavelength,

n_m = n_m(subs) = the effective index of substrate mode, and

n_m(CPW) = the effective index of the CPW coplanar mode (which for Z-cut $LiNbO_3$ = 2.15 at 1.3 μm when optical-microwave phase match is achieved).

It has been known in the prior art that microwave leakage (loss dips in transmission) is due to a microwave coupling between the coplanar mode and a substrate mode bounded by the top and bottom surfaces of the substrate 116. In microwave terminology this is called a surface wave. However, for purposes of this description, the optical terminology of a substrate mode will be used. Although this microwave coupling has been known in the microwave area, it apparently has not been appreciated in the optical modulator area. The frequency at which the microwave coupling, and thus the microwave loss, begins depends on the thickness of the substrate 116 and the dispersion behavior of the substrate mode. It is here where there is a crucial difference

between the use of the coplanar strip (CPS) electrode structure of Figure 2A and the use of a coplanar waveguide (CPW) electrode structure of Figure 2B. It should be recalled that the CPW structure of Figure 2B has ground planes 114A and 114B on both sides of the central electrode 112A, whereas the CPS structure of Figure 2A has a ground plane 114 on only one side of the electrode 112. The dispersion curves for the Z-cut $LiNbO_3$ substrate 116 (shown in inserts 118A and 118B of Figure 3) are different, depending on whether the upper surface of a substrate 116 is coated with the metal 30 (insert 118B) or is not coated with the metal 120 (insert 118A).

Figure 3 shows that the TE_0(die) substrate mode of the non-metal coated substrate 116 of insert 118A occurs at a lower frequency than for the TM_0(cond) substrate mode of the metal coated substrate 116 of insert 118B. From Figure 3, it can be determined that the coplanar mode-substrate mode coupling problem can be solved by using a thick electrode CPW structure (wherein the metal of the thick electrode CPW structure substantially coats the entire top surface) and by making the substrate thickness sufficiently thin that microwave leakage will not occur within the bandwidth of interest. The required thickness of the electrode structure for optical-microwave phase match can be calculated separately by known techniques (to be discussed later).

As stated before, the dispersion curves shown in Figure 3 apply to the specific cases where Z-cut slabs or substrates of $LiNbO_3$ are utilized and air is the material underneath each of the $LiNbO_3$ substrates 116. In these cases the effective index (n_m) of the CPW coplanar mode is adjusted to be close to 2.15.

It will be recalled that microwave leakage (loss dips in transmission) is due to a microwave coupling between the coplanar mode and a substrate mode bounded by the top and bottom surfaces of the substrate 116. To avoid such microwave leakage it is important that the substrate thickness h be sufficiently small at a given λ_0 so that the following equation is satisfied:

$$n_m(\text{subs}) \leq n_m(\text{CPW}) \qquad (1)$$

which for Z-cut $LiNbO_3$ the $n_m(\text{CPW}) = 2.15$ at a wavelength of 1.3 μm when optical-microwave phase match is achieved.

Since h and λ_0 are known, h/λ_0 can be readily calculated and then the effective index of the substrate mode $n_m(\text{subs})$ can be determined from the dispersion curves in Figure 3. For example, if $h/\lambda_0 = 0.04$, then the effective index $n_m(\text{subs})$ of the $TM_0(\text{cond})$ substrate mode for the Z-cut $LiNbO_3$ substrate 116 would be about 2.5. Since $n_m(\text{CPW}) = 2.15$ and $n_m(\text{subs}) = 2.5$, $n_m(\text{subs})$ would not be $\leq n_m(\text{CPW})$ and therefore microwave losses would result when $h/\lambda_0 = 0.04$. To prevent such a microwave loss, h (the substrate thickness) would have to be thinned until the relationship shown in Equation (1) is satisfied across a desired bandwidth. When

this relationship is satisfied, substantially no microwave leakage occurs across that desired bandwidth.

There are several steps that have to be taken to determine the geometry of the broadband, travelling wave, electro-optic integrated optical modulator of the present invention which contains the thick electrode coplanar (CPW) structure on a thin substrate. After the optical index is determined:

1. The coplanar microwave index has to be made equal to the optical index (to be explained in discussion of Figure 9), and

2. Then the substrate must be thinned so that the effective index (or microwave index) of the substrate mode is less than or equal to the effective index (or microwave index) of the CPW coplanar mode. (See Equation (1).)

Referring to Figures 3A and 3B, it will now be explained how the proper thickness can be determined for any suitable Z-cut substrate 119A and for any suitable X- or Y-cut substrate 119B, with each of the substrates 119A and 119B having a metal coating 120 on the upper surface of the substrate. For a more universal application, the following Equations (2) and (3) will also be used in this explanation instead of the dispersion curves of Figure 3.

Equations for Leaky Mode Loss

For the Z-cut case: (TM_0(cond)):

$$\frac{h}{\lambda_0} = \frac{\tan^{-1}\left[\frac{n_e n_0}{n_3^2}\left(\frac{n_m^2-n_3^2}{n_e^2-n_m^2}\right)^{1/2}\right]}{2\pi\left(\frac{n_0}{n_e}\right)\left(n_e^2-n_m^2\right)^{1/2}} \qquad (2)$$

For the X- or Y-cut case: (TM_0(cond)):

$$\frac{h}{\lambda_0} = \frac{\tan^{-1}\left[\frac{n_e n_0}{n_3^2}\left(\frac{n_m^2-n_3^2}{n_0^2-n_m^2}\right)^{1/2}\right]}{2\pi\left(\frac{n_e}{n_0}\right)\left(n_0^2-n_m^2\right)^{1/2}} \qquad (3)$$

where:

h = substrate thickness

λ_0 = free space microwave wavelength

n_0 = ordinary index of substrate

n_e = extraordinary index of substrate

n_m = effective index of substrate mode

n_3 = index of material below substrate

Each of the substrates 119A and 119B respectively utilized in Figure 3A and 3B is a uniaxial crystal which has two indices of refraction, one for fields parallel to Z and the other for fields parallel to X or Y. The Equations (2) and (3) are for the two different orientations of the uniaxial crystal substrates shown in Figures 3A and 3B. More particularly, Equation (2) is for the Z-cut orientation shown in Figure 3A, while Equation (3) is for the X- or Y-cut orientation shown in Figure 3B. In addition, Equation (2) determines the ratio h/λ_0 as a function of the effective index n_m for the TM_0(cond) substrate mode for the Z-cut substrate being used. In a similar manner, Equation (3) determines the ratio h/λ_0 as a function of the effective index n_m for the TM_0(cond) substrate mode for the X- or Y-cut substrate being used.

Assuming that Equation (2) is being utilized during the implementation of the Z-cut substrate for an electro-optic integrated optical modulator of the invention, then the effective index of the CPW coplanar mode n_m(CPW) would be known. In addition, the values h, λ_0, n_0, n_e and n_3 in Equation (2) would also be known. Only n_m or n_m(subs), the effective index of the TM_0(cond) substrate mode, would not be known. By inserting the known values of h, λ_0, n_0, n_e and n_3 into Equation (2), the remaining value of n_m(subs) can be determined and compared with n_m(CPW), the effective index of the CPW coplanar mode, to see if

the relationship shown in Equation (1) [$n_m(subs) \leq n_m(CPW)$] is satisfied. If the relationship is satisfied, then the substrate is thin enough. If the relationship is not satisfied, then h must be thinned until Equation (1) is satisfied.

In a similar manner, if Equation (3) is being utilized during the implementation of the X- or Y-cut substrate for an electro-optic integrated optical modulator of the invention, then the effective index of the CPW coplanar mode $n_m(CPW)$ would be known. In addition, the values h, λ_0, n_0 and n_3 in Equation (3) would also be known. Only n_m or $n_m(subs)$, the effective index of the $TM_0(cond)$ substrate mode, would not be known. By inserting the known values of h, λ_0, n_0 and n_3 into Equation (3), the remaining value of $n_m(subs)$ can be determined and compared with $n_m(CPW)$, the effective index of the CPW coplanar mode, to see if the relationship shown in Equation (1) [$n_m(subs) \leq n_m(CPW)$] is satisfied. If the relationship is satisfied, then the substrate is thin enough. If the relationship is not satisfied, then h must be thinned until Equation (1) is satisfied.

In an earlier experiment, a 10 μm thick electrode CPW structure and a 14 μm thick electrode CPS structure were each fabricated on Z-cut $LiNbO_3$ slabs or substrates 116 with a 0.9 μm thick SiO_2 buffer layer on the substrate. Hot electrode widths were 8 μm, gap widths between a hot electrode and its associated ground plane(s) were 15 μm, and ground planes were 2-3

millimeters (mm) wide. Finite element calculations indicated that those geometries should result in microwave indices near 2.4. These devices were fabricated on substrates 0.5 and 0.25 mm thick and 8 mm wide. The electrode interaction length was 2-4 cm.

The devices were tested on a Hewlett-Packard HP-8510C automatic network analyzer with the electrical transmission (S_{21}) shown in Figure 4A, 4B, 4C and 4D. The CPS devices showed loss dips beginning at 7 GHz for the device with the 0.5 mm thick substrate and at 14 GHz for the device with the 0.25 mm thick substrate. The CPW devices showed similar behavior at about 24 GHz for the device with the 0.5 mm thick substrate, but no significant dips at all out to 40 GHz for the device with the 0.25 mm thick substrate. The frequency at which mode coupling begins is referred to as f_c. For frequencies above f_c, it was verified that microwave power was transmitted to the outer edge of the substrate (parallel to the axis of the device) by perturbing the field at the edge with another slab of $LiNbO_3$, or by sawing off the edge and thus reducing the width of the substrate. These actions had the effect of changing the position of the loss dips with frequency but did not significantly affect f_c. Power was observed at the outer edge of the substrate all along the length of the device. The experimental results (Experiment) for f_c for several devices of each type are listed

in the following TABLE, along with computed (Model) values from Figure 3 assuming $n_m = 2.4$.

TABLE

SUMMARY OF COMPUTED AND MEASURED FREQUENCIES

Device	h (mm)	Substrate mode	f_c(GHz) Model	f_c(GHz) Experiment
CPW	0.5	TM_0 (cond)	25	24-26
	0.25	TM_0 (cond)	49	> 40
CPS	0.5	TE_0 (die)	11	7-8
	0.25	TE_0 (die)	22	14-16

Thus, as shown in Figure 4A and 4C (or Figure 4B and 4D) and the TABLE, for the same thickness substrate the CPS structure shows in Figure 4A (Figure 4B) microwave leakage (loss dips in transmission) at lower frequencies than the CPW structure shows in Figure 4C (Figure 4D).

Figure 5 and 6 respectively show cross-sectional and top views of a high speed phase modulator with coplanar electrodes.

In the phase modulator of Figures 5 and 6, a coplanar waveguide (CPW) structure 111, comprised of a center electrode 113 and ground planes or grounded electrodes 115 and 117 on both sides of the center electrode 113, is disposed on a thin substrate 119 of Z-cut lithium niobate ($LiNbO_3$) to avoid

electrical leakage. Preferably the substrate 119 has a thickness of from 0.16 to 0.24 mm and a width of about 8 mm.

The electrodes 113, 115 and 117 are preferably made of gold and have thicknesses of from 10-20 μm and electrode 113 has an exemplary width of substantially 8 μm. The gap width G between the center electrode 113 and each of the grounded electrodes 115 and 117 is selected to be about 15 μm, while the grounded electrodes 115 and 117 are selected to be about 2-3 mm wide.

The substrate 119 has electro-optic effects, and is coated with an exemplary silicon dioxide (SiO_2) buffer layer 121 having an exemplary thickness of substantially 0.9 μm. In addition, the substrate 119 contains an optical waveguide 125 underneath the electrode 113. The optical waveguide 125 is formed by depositing a strip of titanium (Ti) metal on the surface of the $LiNbO_3$ substrate 119 and diffusing it into the $LiNbO_3$ substrate 119 at high temperature by techniques well known in the art. This is done before the SiO_2 buffer layer 121 and the electrodes 113, 115 and 117 are deposited. Portions of the electrodes 113, 115 and 117 extend in parallel paths over an electrode interaction region of length L (to be explained) which is parallel to the optical waveguide 125. The silicon dioxide buffer layer 121 isolates the optical field in the optical waveguide 125 from the metal electrodes 113, 115 and 117 of the coplanar waveguide structure 111 to prevent optical loss.

It should be noted that the phase modulator of Figure 5 and 6 was fabricated with the above-specified geometries for operation at an exemplary 1.3 μm. Calculations have indicated that these above-specified geometries should result in microwave indices n_m between about 2.2 and about 2.4, as shown in Figure 9 (to be explained).

In operation, 1.3 μm light from a light source 127, such as a laser, is focused by a lens 129 into the optical waveguide 125 and propagates through the optical waveguide 125. At the same time, a modulating microwave drive signal, at an arbitrary amplitude of up to 4 to 5 volts peak and at a frequency in the range from 0 Hz up to substantially 40 GHz, is applied from a microwave source 131 to the coplanar waveguide structure 111 (between an input port 152 on the center electrode 113 and each of the grounded electrodes 115 and 117) and on the same side of the optical modulator as the exemplary 1.3 μm light is transmitted into the optical waveguide 125. The center electrode 113 also includes an output port 153 for termination of the coplanar waveguide structure 111. The low drive voltage of up to 4 to 5 volts peak results in a highly efficient optical modulator. This modulating drive signal modulates the phase of the propagating light or optical wave at the frequency of the microwave drive signal. More particularly, the optical phase modulation results from an interaction between the optical wave

in the optical waveguide 125 and the microwave drive signal in the coplanar waveguide structure 111.

The bandwidth of the phase-modulated optical signal is typically limited by optical-microwave phase mismatch (wherein the microwave wave and the optical wave travel at different velocities, depending on the design of the device). The phase matching or phase velocity matching in the invention will now be discussed.

Since the microwave drive signal and the light waves are both applied on the same side of the optical modulator, the microwave signal and the light waves propagate in the same direction through the electrode interaction region of the modulator. The direction of propagation for both the light waves and the microwave field is into the paper in Figure 5, and from left to right in Figure 6.

The coplanar waveguide structure 111 is designed with the above-discussed geometries so that the microwave field and the light waves propagate with substantially the same phase velocity when the light has a wavelength of about 1.3 μm. When the microwave field and the light waves have the same or matching phase velocities, the phase modulator of Figure 5 and 6 has the best broadband response characteristics.

The phase velocity match is determined by the effective indices of the optical and microwave field modes. The effective

index of the optical mode is fixed by the index of refraction of the substrate 119. The effective index of the microwave field in the coplanar waveguide structure is determined by the geometry of the electrode structure of the optical modulator of Figures 5 and 6, the width W of the center electrode 113, the gap G between the center electrode 113 and each of the grounded electrodes 115 and 117, the height H and geometry of the electrodes 113, 115 and 117, the material and the dielectric constants of the buffer layer 121 and the substrate 119, and the thickness of the silicon dioxide buffer layer 121. These parameters are selected to make the effective index of the microwave field mode as close as possible to the effective index of the optical mode.

Of particular importance in producing a phase velocity match in the invention is the use of a thick electrode structure (of from 10-20 μm) on a coplanar waveguide (CPW) structure 111 (wherein the metal of which substantially coats the entire top surface of the buffer layer-coated substrate 119, as indicated in Figure 5 and 6) and the use of a substrate 119 having a thickness sufficiently thin (preferably of from 0.16 to 0.24 mm) so that microwave leakage will substantially not occur within the bandwidth of interest (up to 40GHz).

Referring now to Figure 7 and 8, Figures 7 and 8 respectively show cross-sectional and top views of a high speed intensity modulator with coplanar electrodes. This design is the

exemplary design for the intensity modulators M_1 and M_2 used in the mixer 10 of Figure 1. Figure 7 and 8 are respectively substantially the same as Figure 5 and 6, except that they are cross-sectional and top views of a high speed Mach Zehnder interferometer modulator instead of just the phase modulator of Figure 5 and 6. The Mach Zehnder interferometer modulator of Figure 7 and 8 produces an intensity modulation at its output.

The Mach-Zehnder interferometric modulator of Figure 7 and 8 is fabricated in a manner similar to the fabrication of the phase modulator of Figure 5 and 6. More particularly, the Mach-Zehnder interferometer is used with a coplanar waveguide (CPW) structure 111 on a thin substrate 119 of z-cut $LiNbO_3$ to avoid electrical leakage. The thickness of gold electrodes 113, 115 and 117 are varied from 10-20 μm. The substrate 119 is coated with a 0.9 μm SiO_2 buffer layer 121. The widths of the electrode 113 is 8 μm, the gap widths G are 15 μm and the ground planes 115 and 117 are 2-3 mm wide. In addition, the optical waveguide 125 of Figure 5 is replaced by optical waveguide arms 125A and 125B respectively disposed in the substrate 119 respectively underneath the center electrode 113 and the ground plane or grounded electrode 117, as shown in Figure 7. The optical waveguide arms 125A and 125B are formed by selectively applying strips of Ti metal on the surface of the $LiNbO_3$ substrate 119 and diffusing them into the $LiNbO_3$ substrate at room temperature by techniques well known in the

art. This is done before the SiO_2 buffer layer 121 and the electrodes 113, 115 and 117 are deposited on the substrate 119.

The optical waveguide arms 125A and 125B are optically coupled together at one end to an input waveguide 125C and at a second end to an output waveguide 125D to form a Mach-Zehnder interferometer configuration, as shown in Figure 8.

It should be noted that the Figure 5-8 are shown for a Z-cut $LiNbO_3$ substrate, where the Z-axis is normal to the plane of the $LiNbO_3$ substrate. (See insert 118A in Figure 3.) For an X- or Y-cut $LiNbO_3$ substrate 119 in Figure 5, the optical waveguide 125 would be similarly formed in the substrate 119 (as discussed before), but it would be located between the center electrode 113 and one of the grounded electrodes 115 and 117. Similarly, for an X- or Y-cut $LiNbO_3$ substrate 119 in Figure 7, the optical waveguide arms 125A and 125B would be similarly formed in the substrate 119 (as discussed before), but the waveguide arm 125A would be located between the center electrode 113 and the grounded electrode 115, while the waveguide arm 125B would be located between the center electrode 113 and the grounded electrode 117.

The operation of the embodiment of Figure 7 and 8 is substantially the same as the operation of the embodiment of Figure 5 and 6, with the following exceptions. Light at the exemplary 1.3 μm wavelength applied to optical waveguides 125A

and 125B is preferably polarized light with orientation appropriate to the type of substrate and to the type of cut (such as X-cut, Y-cut or Z-cut). For example, an intensity modulator using a z-cut $LiNbO_3$ substrate 119 provides optimal response to vertical polarized light. The light from the light source 127 is most preferably cw laser light. It may be focused by the lens 129 into the input waveguide 125C or may be transmitted via an optical fiber, preferably a polarization-maintaining fiber. The light from the light source 127 is divided into the optical waveguide arms 125A and 125B of the interferometer. At the same time, a modulating microwave drive signal, at an arbitrary amplitude of up to the drive voltage V_π and at a frequency in a preselected range, is applied from the microwave source 131 to the coplanar waveguide structure 111 (between the input port 152 on the center electrode 113 and each of the grounded electrodes 115 and 117) and on the same side of the optical modulator as the exemplary 1.3 μm light is transmitted into the optical waveguide 125. The center electrode 113 also includes an output port 153 for termination of the coplanar waveguide structure 111. As discussed further below, the drive voltage V_π is also known as the half-wave voltage V_π, which is the change in microwave voltage applied to the input port 152 which results in phase reversal, i.e. phase shift by a half-wave, i.e. phase shift by π radians. The half-wave voltage $V_\pi(f)$ generally increases with

frequency of the applied microwave signal and is typically on the order of no more than 4 to 5 volts for DC. The preselected frequency range can be as high as from 0 Hz up to substantially 40 GHz.

The modulating drive signal modulates the light or optical waves in the waveguide arms 125A and 125B. The light in the two arms 125A and 125B is phase shifted in opposite directions before it is recombined in the output waveguide 125D to produce an output beam which contains intensity or amplitude modulation. It is the modulating microwave drive signal which modulates the intensity of the light in the interferometer at the frequency of the microwave drive signal. More particularly, the optical intensity or amplitude modulation results from an interaction between the optical wave in the optical waveguides 125A and 125B and the microwave drive signal in the coplanar waveguide structure 111.

The object of velocity matching in the invention is to implement the optical phase modulator of Figures 5 and 6 or the optical intensity modulator of Figure 7 and 8 so as to cause the velocity of the microwave wave to be the same as or substantially equal to the velocity of the optical wave. That will result in an improved optical response for the optical modulator. The velocity of the optical wave is the velocity of light divided by the

optical index, while the velocity of the microwave wave is the velocity of light divided by the microwave index.

Three different optical modulator devices were fabricated on substrates 119 that were 0.16-0.25 mm thick and 8 mm wide and with the remaining geometries specified above for the embodiment of Figures 7 and 8. More specifically, as indicated in Figure 9, the thicknesses of the electrodes 113, 115 and 117 on each of the substrates 119 (and the associated microwave indices) of the three above-noted optical modulators were about 11.5 μm (and about 2.44 n_m), about 14.6 μm (and 2.37 n_m) and about 18 μm (and about 2.29 n_m). The electrode interaction length L_1 (Figure 8) was 24 mm. Finite element calculations indicated that these geometries should result in microwave indices n_m between 2.2 and 2.4, as shown in Figure 9. Figure 9 will now be discussed.

Figure 9 illustrates a plot of the CPW microwave index n_m against electrode thickness, and a comparison of theoretical results with experimental results. More specifically, Figure 9 shows the optical index at 2.15, as represented by the horizontal line 141. Figure 9 also shows a calculated version of a coplanar waveguide microwave (or effective) index of the CPW coplanar mode, as represented by the sloping line 143, as a function of the thickness of the electrodes 113, 115 and 117 for the above-specified geometries. Figure 9 also shows three data points 145, 147 and 149 for the above-noted three fabricated devices of

different electrode thicknesses. Note that the microwave index of each of these data points 145, 147 and 149 decreases as the associated electrode thickness increases. Figure 9 shows how well each of the three devices is velocity matched. Note that the line 141 (representing an optical index of 2.15) and the line 143 (representing the CPW microwave index vs. electrode thickness of the electrodes 113, 115 and 117) intersect at about an electrode (113, 115 and 117) thickness of about 20 μm. An exact velocity match would be at a microwave index of 2.15, which is the optical index for a wavelength of 1.3 μm. Thus, to obtain an exact velocity match, the coplanar waveguide microwave (or effective) index 143 has to be made equal to the optical index 141. As shown in Figure 9, this occurs at the point 144 where the lines 141 and 143 intersect.

The coplanar microwave index of the CPW coplanar mode for a given geometry of the electrode structure is determined by the thickness of the electrodes 113, 115 and 117. Therefore, the electrodes 113, 115 and 117 must be thick enough so that the coplanar waveguide microwave index is equal to the optical index in the uniaxial crystal (which is 2.15 in $LiNbO_3$). However, it should be realized that an exact velocity match could be obtained for a different optical index (for a different wavelength and/or for a different crystal material) by following a similar procedure.

The optical modulator of the invention can be implemented to operate with any optical wavelength, but the above-discussed optical modulators of the embodiment of Figure 5 and 6 and the embodiment of Figure 7 and 8 were implemented to operate at an optical wavelength of 1.3 μm.

Referring now to Figures 10A and 10B, Figure 10A illustrates the electrical transmission through the coplanar microwave waveguide structure 111 (Figure 7 and 8 or Figure 5 and 6); and Figure 10B illustrates the normalized optical response of the device of Figure 5 and 6 or of Figure 7 and 8 in dB of electrical power as a function of frequency.

Figure 10A shows that the magnitude of S_{21} in dB plotted against frequency over the frequency range from 0 Hz to 40 GHz, where S_{21} is a transmission parameter from a network analyzer used in the measurement. Figure 10A basically indicates what the transmission of the optical modulator of the invention is in dB as a function of frequency.

Figure 10B shows the normalized response of the optical modulator of the invention in dB of electrical power, not optical power, as a function of frequency over the frequency range from 0 Hz to 40 GHz. Experimental data points are shown about a theoretical normalized optical response line 151. Note that the normalized optical response decreases with an increase in frequency. With a velocity matched optical modulator the drop off

with frequency will be minimized. Ideally a flat response over the frequency range from 0 Hz to 40 GHz is desired. However, Figure 10B shows that the optical modulator of the invention that was tested only dropped about 7.5 dB over the frequency range from 0 Hz to 40 GHz, which is a very good response.

Therefore, what has been described in preferred embodiments of the invention is a broadband, electro-optic modulator which, in an embodiment shown in Figures 5 and 6 comprises: a substrate having substrate modes, having electro-optic effects, and having a first optical waveguide adapted to receive and transmit light therethrough in a first direction and with a first phase velocity; a buffer layer disposed on the substrate; and a coplanar waveguide electrode structure having a coplanar mode and being disposed on the buffer layer for receiving an electrical signal propagating therethrough in the first direction with a second phase velocity to phase modulate the light in the optical waveguide at a frequency in the range from 0 Hz up to substantially 40 GHz. The substrate has a sufficiently small thickness so that coplanar-substrate coupling substantially does not occur over a desired frequency bandwidth of operation, and the coplanar waveguide electrode structure has a sufficiently large thickness so that the second phase velocity of the electrical signal is substantially equal to the first phase velocity. In an embodiment shown in Figures 7 and 8, an intensity

modulator is produced by adding a second optical waveguide which, in combination with the first optical waveguide, forms an interferometer. The interaction of the electrical signal with the optical signal produces an intensity-modulated optical beam. This exemplary modulator is described further in G.K. Gopalakrishnan et al, "Electrical Loss Mechanisms in Travelling Wave $LiNbO_3$ Optical Modulators," Electronics Letters, Vol.28, No.2, pp. 207-208 (16 Jan. 1992) and in G.K. Gopalakrishnan et al, "40 GHz, Low Half-Wave Voltage Ti:$LiNbO_3$ Intensity Modulators," Electronics Letters, Vol.28, No.9, pp. 826-827 (23 April 1992), which articles are incorporated herein by reference.

The above-described exemplary intensity modulator is a traveling wave modulator, as distinguished from a lumped element modulator. As discussed in L.M. Johnson, "Relative Performance of Impedance-Matched Lumped-Element and Traveling-Wave Integrated-Optical Phase Modulators," (IEEE Photonics Technology Letters, Vol. 1, No. 5, May 1989, pp. 102-104), which is incorporated herein by reference, a lumped element modulator is modeled as and characterized by resistance and capacitance and by an impedance which varies with electrical frequency. A traveling wave modulator is modeled as and characterized by an impedance which is relatively independent of electrical frequency. Lumped element modulators are typically bound with wires to other components; traveling wave modulators are typically part of

microwave transmission lines. The former type of modulator is typically more effective at lower frequencies (say, below 1 megaHertz (MHz)) than at higher frequencies, and the latter type of modulator is typically more effective at higher than at lower frequencies.

The above-described exemplary intensity modulator is considered broadband, since it has good response over a preselected frequency range on the order of tens of GHz.

Having described the invention in general, the following example is given as a particular embodiment thereof and to demonstrate the practice and advantages thereof. It is understood the example is given by way of illustration and is not intended to limit the specification or the claims to follow in any manner. This example is discussed further in G.K. Gopalakrishnan et al, "A $LiNbO_3$ Microwave-Optoelectronic Mixer with Linear Performance," 1993 IEEE MTT-S Digest, Conference Proceedings, International Microwave Symposium, Atlanta, Ga., pp. 1055-1058; G.K. Gopalakrishnan et al, "Microwave-Optical Mixing in $LiNbO_3$ Modulators," IEEE Transactions on Microwave Theory and Techniques, Vol. 41, No.12, pp. 2383-2391 (December 1993), which articles are incorporated herein by reference.

Referring now to Figure 11, the above described exemplary

modulators M_1 and M_2 may include biasing means 180 and 190, respectively. For each of the modulators M_1 and M_2, a DC bias voltage S_{dc1} and S_{dc2} is applied to a bias T-connector 200 and 210, respectively. An isolator 220 and 230 is coupled between the microwave signal producer 20 and the bias T-connector 200 and 210, respectively. As a result, the biasing means 180 and 190 produce biased microwave signals S_1' and S_2' for input to the input ports 152_1 and 152_2 of modulators M_1 and M_2, respectively.

Referring back to Figures 7 and 8, the modulators M_1 and M_2 are designed for operation at an optical wavelength of 1.3μm with the characteristic impedance of the CPW line (Z_0) being approximately 35 ohms (Ω). They are fabricated as follows: The electrodes 113, 115 and 117 are preferably made of gold and have thicknesses of 15 and 18μm, respectively. The electrode 113 has a width of 8 μm. The gap width G between the center electrode 113 and each of the grounded electrodes 115 and 117 is selected to be 15 μm, while the grounded electrodes 115 and 117 are selected to be about 2-3 mm wide. The substrate 119 has a width of 8 mm and a thickness of from 0.2 to 0.15 mm for modulators M_1 and M_2, respectively. The electrode interaction length L_1 was 24 mm. The substrate 119 is coated with a 0.9 μm SiO_2 buffer layer 121.

As so fabricated, the modulators M_1 and M_2 have DC half-wave voltages V_π of 4.2 and 5 Volts, respectively. When biased for

maximum transmission, the optical insertion loss through each modulator is approximately 4dB.

The above-described exemplary intensity modulator is considered a low drive voltage modulator since the DC drive voltage $V_\pi(DC)$ is below about 5 Volts. The significance of the modulator being a low drive voltage modulator is discussed further below.

From a fit to the electrical response of the modulator comprising conductor, dielectric and radiative losses and considering the microwave-optical index mismatch (0.06 for modulator M_1 and 0.128 for modulator M_2) obtained from a fit to the optical response, the modeled optical responses of the modulators M_1 and M_2 are shown in Figure 12. Referring back to Figure 11, the model also takes into consideration reflections that occur at the transition from the 35Ω CPW line to the 50Ω load 240 and 250 at the output ports 153_1 and 153_2, respectively. Here, a concern is to characterize traveling wave modulators in terms of their mixing efficiency. A fundamental mixer parameter that reflects mixing efficiency is its RF conversion loss. As will be discussed further later, the RF half-wave voltage $V_\pi(f)$ of the modulators M_1 and M_2, adequately characterizes the mixing efficiency of the modulators M_1 and M_2. The RF half-wave voltage $V_\pi(f)$ of the modulators M_1 and M_2 may be obtained from the optical

response of the modulators M_1 and M_2 by using the following expression:

$$V_\pi(f) = V_\pi(DC) \cdot \left[\frac{Z_0 + Z_D}{2Z_D}\right] \cdot 10^{-OR/20}, \quad (4)$$

where $V_\pi(DC)$ is the half-wave voltage of the modulator at DC, Z_0=50Ω is the characteristic impedance of the line, Z_D is the characteristic impedance of the CPW electrode of the device, and OR is the optical response of the modulator in electrical decibels. Also shown in Figure 12 are the modeled RF half-wave voltages $V_\pi(f)$ of M_1 and M_2 as a function of frequency f.

Referring back to Figure 11, the above-described exemplary pair of interferometric modulators M_1 and M_2 are cascaded in series, and down-conversion is demonstrated. This is done by applying a single-tone RF input S_1 of angular frequency ω_1 to one modulator M_1, the modulated optical output L_{m1} of which is mixed with a larger LO local oscillator pump signal S_2 of angular frequency ω_2 applied to the other modulator M_2. The modulator M_2 produces a second modulated optical signal L_{m2} having an angular frequency component at IF, i.e. the difference $|\omega_1-\omega_2|$ between the angular frequencies ω_1 and ω_2. The second modulated optical signal L_{m2} is detected with a photoreceiver 260, the output of

which is applied to a spectrum analyzer 270 having a 50Ω load. The second modulated optical signal L_{M2} produced by the modulator M_2 also has an angular frequency component at the sum $\omega_1+\omega_2$ of the angular frequencies ω_1 and ω_2, but his component is not as relevant to down-conversion applications as the IF component.

The actual signals that take part in the mixing are optical signals (not shown) at the RF (ω_1) and LO (ω_2) frequencies, derived from electrical inputs S_1' and S_2', respectively, applied to modulators M_1 and M_2, respectively. To efficiently down-convert these to a desired IF, optical signals at both the RF and LO frequencies must be highly modulated, and, hence, to prevent leakage of power to other unwanted frequencies, both modulators M_1 and M_2 should be biased at quadrature.

In this configuration, the intended application of the cascaded modulator pair M_1-- M_2 is for antenna remoting. Antenna remoting usually refers to an arrangement of source, fiber coupled remote (from the source and often from electrical power) modulator, and fiber coupled detector (usually located with the source). The RF signal from the detector is then usually electrically down-converted in a mixer and processes.

Upon application of this invention to antenna remoting, the RF signal is fed to one modulator, say, M_1 and the local oscillator LO to the other, say, M_2, with the modulator receiving the RF signal considered the remote modulator. The mixing

process provides down-conversion, and only the IF needs to be detected. For such an application, one modulator M_1 can be used to transmit the relatively low-power RF-modulated optical signal L_{m1} from a remote location over an optical fiber. The RF signal can then be down-converted by mixing the RF-modulated optical signal L_{m1} with a relatively large LO pump signal S_2 applied to the other modulator M_2. Electrical mixing is no longer needed and the weak points of conventional microwave mixers, described earlier, are eliminated. The advantages of this approach for antenna remoting are that the IF is obtained directly at the detector, thus reducing demands on the detector, since the detector does not need to be broadband, and that the mixing is accomplished optically with broad bandwidth, on the order of tens of GHz, and with infinite port-to-port isolation.

This tandem arrangement of modulators M_1 and M_2 also allows for multiplication of RF signals applied to each modulator, and to up-conversion of RF signals applied to each modulator.

For a single Mach-Zehnder interferometer modulated by electrical RF signal $V \cdot \sin(\omega t)$ and having half-wave voltage V_π, the normalized ratio of output optical power P_o to input optical power P_i is

$$\frac{P_o}{P_i} = \frac{1}{2}\left(1+\cos\left[\phi_0+\frac{\pi V}{V_\pi}\right]\right), \qquad (5)$$

where ϕ_0 is the intrinsic phase bias. In this derivation, each interferometer M_1 and M_2 is biased at quadrature, so $\phi_0=90^\circ$.

If RF input signals $S_1 = V_1 \cdot \sin(\omega_1 t)$ and $S_2 = V_2 \cdot \sin(\omega_2 t)$ are applied to modulators M_1 and M_2, respectively, each biased at quadrature, then using equation (5), the ratio of the output optical power P_o of the signal L_{m2} to the input optical power P_i of the source light L_i is

$$\frac{P_o}{P_i} = \frac{T_D}{4}\left(1+\cos\left[\frac{\pi}{2}+\frac{\pi V_1}{V_{\pi 1}(\omega_1)}\right]\right)\cdot\left(1+\cos\left[\frac{\pi}{2}+\frac{\pi V_2}{V_{\pi 2}(\omega_2)}\right]\right), \qquad (6)$$

where T_D is the coupling and optical transmission losses of the system and $V_{\pi 1}(\omega_1)$ and $V_{\pi 2}(\omega_2)$ are the RF half-wave voltages of modulators M_1 and M_2 at angular frequencies ω_1 and ω_2, respectively. Rewriting and expanding equation (6) and neglecting terms higher than third order, we get:

$$\frac{P_o}{P_i} = \frac{T_D}{4}\,(1-[2J_1(X_1)\sin\omega_1 t+2J_3(X_1)\sin3\omega_1 t] - [2J_1(X_2)\sin\omega_2 t+2J_3(X_2)\sin3\omega_2 t] + [2J_1(X_1)\sin\omega_1 t+2J_3(X_1)\sin3\omega_1 t] \cdot[2J_1(X_2)\sin\omega_2 t+2J_3(X_2)\sin3\omega_2 t]\,), \tag{7}$$

where J_n is the Bessel function of order n, $X_1=(\pi\cdot V_1)/(V_{\pi 1}(\omega_1))$, and $X_2=(\pi\cdot V_2)/(V_{\pi 2}(\omega_2))$.

From Equation (7), for $X_1\ll 1$ and $X_2\ll 1$, neglecting power terms higher than third order, we get

$$\frac{P_o}{P_i} = \frac{T_D}{4}\,(1- X_1\sin\omega_1 t - X_2\sin\omega_2 t - \frac{X_1^3}{24}\sin3\omega_1 t - \frac{X_2^3}{24}\sin3\omega_2 t + \frac{X_1X_2}{2}\,[\cos(\omega_1-\omega_2)\,t - \cos(\omega_1+\omega_2)\,t]\,). \tag{8}$$

In equation (8), the terms associated with the third harmonic frequencies ($3\omega_1$ and $3\omega_2$) are small compared to the fundamental, sum and difference terms and hence can be neglected. It can be seen from the above derivation of equation (8) that the third order IM frequency terms ($2\omega_1-\omega_2$ and $2\omega_2-\omega_1$) are not present when each interferometer of the cascaded pair M_1--M_2 is biased at quadrature. In conventional mixers, if $\omega_1\approx\omega_2$, then the IM frequencies would be very close to the signal frequencies and thus could not be filtered out. However, as shown, the present

invention has low IM distortion. Furthermore, the power associated with the IM frequencies is proportional to the cube of the input voltages V_1 and V_2, so the power increases rapidly with input power thereby limiting the dynamic range of the mixer 10. The cascaded Mach-Zehnder interferometric pair M_1--M_2, when biased at quadrature, does not suffer from such drawbacks and hence is an attractive candidate for microwave-optoelectronic mixing.

The electrical power delivered by the photodetector 260 to the 50Ω load for angular frequencies $\omega_1-\omega_2$ and $\omega_1+\omega_2$ can be evaluated using the following expression:

$$P(\omega_1 \mp \omega_2) = L(\omega_1 \mp \omega_2) \frac{I_{DC}^2}{2} (2J_1(X_1) \cdot J_1(X_2))^2 \cdot 50 , \qquad (9)$$

where $L(\omega)$ collectively represents angular frequency dependent losses such as detector roll-off and cable losses that limit the performance of the fiber-optic link, and I_{DC} is the detected DC photocurrent.

To demonstrate the effect of quadrature biasing on IM distortion, the modulators M_1 and M_2 were biased off-quadrature, and equal amplitude input signals at f_1=15.52GHz (RF) and f_2=15.56GHz (LO) were applied to the modulators M_1 and M_2,

respectively. The output spectrum, in addition to the signal terms f_1 and f_2, contains the following beat signals: the desired IF difference signal at f_2-f_1=40MHz, and the undesired intermodulation signals at $2f_1-f_2$=15.48GHz and $2f_2-f_1$=15.6GHz. This is illustrated in Figure 13, where the spectra of the signal and IM frequencies are shown. However, when each device M_1 and M_2 of the cascaded pair is biased at quadrature, the IM signals disappear, resulting in optical signals at just the signal and difference frequencies, as illustrated in Figure 14. Since the mixer 10 conserves optical power, the less the power of output IM signals, the greater the power of output sum and IF signals, and therefore the more efficient the mixer 10 is. The mixer 10 in which modulators M_1 and M_2 are biased at quadrature is a more efficient mixer. In comparing Figures 13 and 14, it can be seen that more power is output in the sum and IF frequencies when the modulators M_1 and M_2 are biased at quadrature.

To demonstrate that the IF can be anywhere in the broadband DC to 40GHz frequency range, the experiment was extended to higher frequencies. Signals S_1 and S_2 at frequencies f_1=15GHz and f_2=6GHz were applied to the modulators M_1 and M_2, respectively and the mixer 10 produced the IF difference signal at 9GHz.

For input signals at f_1=15.52GHz (RF) and f_2=15.56GHz (LO), Figure 15 shows the variation of detected IF power at 40MHz with input RF power for a detected DC photocurrent of 0.05mA; the LO

pump power was varied from -20 to +20dBm (0.01mW-100mW). At these values of RF and LO, $V_{\pi 1}(f_1)$=7.7V and $V_{\pi 2}(f_2)$=8.9V. Since the IF was at 40MHz, $L(\omega)$ is negligible. Here, with the LO pump power at +20dBm, the conversion loss is approximately 66dB. At 40GHz (f_1=40.02GHz, f_2=40.06GHz; $V_{\pi 1}(f_1)$=10.4V and $V_{\pi 2}(f_2)$=14.2V), the corresponding computed results are shown in Figure 16 and the conversion loss in this case for a pump power of +20dBm is about 72 dB. Here, the relatively large conversion loss is attributable in part to the optical insertion loss of the interferometric pair M_1--M_2. We were limited to approximately 12mW of optical power from the laser at the input to the first modulator M_1. At the output, for a detected DC photocurrent of 0.05mA, the power striking the detector 260 was 0.1mW (assuming a detector responsivity of 0.5 Amp/Watt) indicating an optical link loss in excess of 20 dB. Here, the modulators M_1 and M_2 biased at quadrature contribute to 14dB (approximately 7dB each) of this loss, and coupling losses account for the rest.

The conversion loss of the cascade interferometric pair M_1--M_2 would be significantly lower if the power on the photodetector 260 were larger. This may be accomplished by employing more powerful lasers 32, or by employing erbium doped fiber amplifiers (EDFA). In this context, we note again that the optical LO pump signal in our experiments was derived by applying a large electrical input to the modulator. If this input were

increased further, then beyond a certain point, compression of the output would occur due to sinusoidal modulator response. In other words, for amplitude greater than the half-wave voltage $V_\pi(f)$, the modulation would swing over more than a half-wave. However, with erbium doped fiber amplifiers (EDFA) currently becoming available at an optical wavelength of 1.5μm, a better way to generate this optical pump signal would be, as shown in Figure 19, to employ an EDFA 280 to amplify the modulated optical LO pump signal L_{m1} which could then be mixed with a lower RF signal S_2 to accomplish down-conversion. Alternatively, as shown in Figure 20, an EDFA 280 could be employed to amplify the output IF signal.

The mixing efficiency of the interferometric pair for RF down-conversion is dependent on the strengths of the modulated optical RF and LO signals. It is, therefore, of interest to study optical modulation at the RF and LO signal frequencies. Towards this end, we applied two independent equal amplitude signals S_1 and S_2 spaced 40MHz apart to the cascaded interferometric modulator pair M_1--M_2 biased at quadrature; the frequencies were centered around 15.5 GHz. For the modulating RF input corresponding to modulator M_1, we show in Figure 17 the variation of the detected signal power as a function of input RF power, for a photodetector 260 current of 0.05mA. for this measurement, $L(\omega)$=-3dB. As shown, this data is in fairly good

agreement with theory with the output increasing linearly with input for power levels that do not cause compression. Also shown, the computed response at 40GHz assuming the same DC photocurrent and the same $L(\omega)$. In actuality, however, the signal strength at 40GHz would be smaller than that predicted because $L(\omega)$ would be worse than -3dB.

The significance of the exemplary modulators M_1 and M_2 having low drive voltage V_π is in relation to conversion loss. The conversion loss is a fundamental mixer parameter employed to define the mixing efficiency. Conversion loss (CL) is defined as follows:

$$\text{RF CL (dB)} = \text{detected IF power (dBm)} - \text{input RF power (dBm)}. \quad (10)$$

The lower the conversion loss, the larger the detected down-converted IF signal strength, and hence the better the signal to noise ratio. For the first signal S_1 being the RF signal, and the second signal S_2 being the LO signal, equation (9) becomes:

$$P(RF \mp LO) = L(RF \mp LO) \frac{I_{DC}^2}{2} (2J_1(X_{RF}) \cdot J_1(X_{LO}))^2 \cdot 50 . \quad (11)$$

In equation (11), the input RF power is contained in the $J_1(X_{RF})$ term, and the LO pump power is contained in the $J_1(X_{LO})$ term. The

laser power is contained in the I_{DC} term. Employing the small-signal argument for the Bessel function, it can be seen that the detected IF (|RF-LO|) output power is inversely proportional to the <u>fourth</u> power of the frequency dependent half-wave voltage V_π of the modulators M_1 and M_2, and is directly proportional to the square of the detected DC current. Thus, the conversion loss of the mixer 10 can be decreased by either increasing the detected optical signal power, such as by employing high power lasers or optical amplifiers, or by employing modulators with lower half-wave voltages. A small decrease in half-wave voltage V_π 33% results in the detected power being multiplied by a disproportionally large factor. For example, a decrease in half-wave voltage V_π by 33% results in the detected power being multiplied by a factor of $(3/2)^4 = 2.5$. The modulator discussed in D.W.Dolfi et ano., "40 GHz Electro-Optic Modulator with 7.5V Drive Voltage," Electronics Letters, Vol. 24, No. 9, pp. 528-529 (April, 1988) discusses a modulator having DC half-wave voltage of 7.5 V. As discussed above, the exemplary modulators M_1 and M_2 herein have DC half-wave voltage of about 5V. Therefore, the mixer disclosed herein has detected power of about 2.5 times the detected power of the mixer disclosed in Johnson '086 using the modulators of Dolfi, supra.

Referring now to Figure 18, the conversion loss in decibels is plotted against the RF Half-Wave voltage $V_\pi(f)(RF)$. As shown,

the conversion loss increases rapidly as the RF half-wave voltage increases. The modulator discussed in Dolfi (supra) exhibits an RF half-wave voltage of 24V. Thus, for a detected DC photocurrent of 1 milliAmp (mA) and a LO pump power of 20 dBm (100 milliWatts (mW), a cascade-connected pair of such modulators would provide a conversion loss of about 55 dB. The above-described exemplary modulator has an RF half-wave voltage of 10.4V, and so the mixer shown in Figs. 1 and 11 would have a conversion loss of about 43dB, 12 dB better than Dolfi. A further improvement of 20 dB could be obtained if the detected photo-current could be increased to 10mA with a more powerful laser or optical amplifier, as discussed further below. Overall, a conversion loss of less than about 40dB provides a practical mixer. In systems with higher conversion losses, the modulated signal would be masked by noise.

For a detected photo-current of 0.05mA, the measured signal-to-noise ratio of the mixer described herein in which amplifiers are not employed at the output is about 37dB for IF at 9GHz, and about 40dB for IF at 40MHz. These measurements reflect the noise of the spectrum analyzer 270.

In a fiber optic link, baseband information is transmitted over an optical fiber from the transmitter end to the receiver end, which recovers the baseband information.

Referring now to Figure 21, an exemplary fiber optic link transmission system 290 is based on the above-described mixer (Figure 1). This exemplary transmission system 290 is discussed further in G.K. Gopalakrishnan et al, "A Fiber-Optic Link for Microwave Subcarrier Transmission and Reception," 1995 IEEE MTT-S Digest, Conference Proceedings, International Microwave Symposium, Orlando, Fla., pp.1165-1168 (May 15-19 1995).

The fiber link transmission system 290 includes first and second optical interferometric modulators M_1 and M_2, each preferably being broadband, traveling-wave intensity modulators having DC drive voltage below about 5V, and most preferably Ti:$LiNbO_3$ traveling-wave intensity modulators as described above. The first modulator M_1 is driven by polarized light L_i, and most preferably polarized cw laser light L_i produced by device 30.

A baseband source 300 produces the baseband information signal S_i. An exemplary baseband signal S_i used for test purposes is a 50 Mbit/s non-return-to-zero $(2^{23}-1)$ pseudo-random bit stream from the data transmitter of a bit error rate (BER) test set which is amplitude shift keyed (ASK). The baseband information signal S_i is preferably, but not necessarily digital, and is not necessarily modulated. Other forms of modulation and especially pulse code modulation known in the art may be used, such as frequency shift keyed (FSK), phase shift keyed (PSK), quaternary phase shift keyed (QPSK), and quadrature amplitude

modulation (QAM). The baseband information signal S_i is applied to the IF port of an electrical microwave mixer M_o^e and upconverted to the microwave frequency band by application of a microwave signal S_{rf} of frequency f_{rf} produced by an RF synthesizer 310 and applied to the RF port of the mixer M_o^e. The frequency f_{rf} for the microwave signal S_{rf} is the subcarrier frequency and exemplary subcarrier frequencies f_{rf} are 9GHz and 16GHz. Microwave modulators M_o^e with performance to 75GHz have been demonstrated, so the technique advanced herein could easily be extended to higher subcarrier frequencies.

The electrical output of the mixer M_0^e is applied to the first optical modulator M_1 as signal S_1". Although the mixer M_0^e output could be applied to the first optical modulator M_1 by standard microwave transmission means, it could also be transmitted in free space to the modulator M_1. Thus, the mixer M_0^e and modulator M_1 could be remote from each other and the transmission system 290 could be used in wireless communications.

The first optical modulator M_1 responsive to the signal S_1" and the source light L_i responsively produces a first modulated optical signal L_{m1}. This first modulated optical signal L_{m1} is responsive to the upconverted signal S_1" and so the process described so far involves subcarrier modulation with subcarrier frequency f_{rf} determined by the microwave signal S_{rf}.

The upconverted signal L_{m1} is transmitted, preferably but not necessarily by polarization-maintaining means 40, and most preferably polarization-maintaining optical fiber (PMF) 40, to the second modulator M_2. The second modulator M_2 is disposed apart from and may be some distance from the first modulator M_1. The second modulator M_2 is cascade coupled to the first modulator M_1 and responsive to the first modulated signal L_{m1} and to a second electrical microwave signal S_2'' for producing a second modulated optical signal L_{m2} having a component with frequency at the difference between the frequencies of the electrical signals S_1'' and S_2'' respectively. The second electrical microwave signal S_2'' is an LO pump signal produced by an LO synthesizer 320. The second modulator M_2 thus performs downconversion. In particular, the subcarrier frequency f_{IF} of the second modulated optical signal L_{m2} is the difference between f_{rf} and the frequency of S_2'', say, f_{IF}=200MHz.

The second modulated optical signal L_{m2} is detected by a photoreceiver 260 with exemplary bandwidth of 300MHz. Photoreceivers 260 with bandwidths as high as 10GHz are presently available and could just as readily be used. The electrical output of photoreceiver 260 is then processed to recover the baseband data as a signal S_0.

The photoreceiver 260 need only have sufficient bandwidth to detect the IF subcarrier and recover the baseband information.

Because of downconversion by the second optical modulator M_2, it is not necessary for the photoreceiver 260 to be of high enough speed to detect the subcarrier frequency f_{rf}. Therefore, the problems associated with high speed photodetectors are avoided.

An exemplary system for recovering the baseband data includes a 150 MHz high-pass filter (HPF) 330 and an amplifier 340 for amplifying the signal by about 30 dB. The output of the amplifier 340 and an IF signal at the frequency f_{IF} produced by an IF synthesizer 350 are mixed by an electrical mixer M_3^e to produce the output information signal S_0.

Optionally, to avoid potential subcarrier and clock recovery, the RF synthesizer 310, LO synthesizer 320, and IF synthesizer 350 are phase locked to a 10MHz reference provided by a reference source 355.

For purposes of testing the apparatus 290, the output signal S_0 was filtered with a 50MHz low pass filter 360 and applied to an error detector 370 of the BER test set.

Referring now to Figure 22, The BER as a function of received optical power is shown for two different carrier frequencies (9 and 16 GHz). Error free transmission (corresponding to a BER of less than 10^{-9} was achieved at received optical powers of $\geq$-30.5 dBm at 9 GHz and $\geq$-28.5 dBm at 16 GHz. When the carrier frequency is increased from 9 to 16 GHz, there is a power penalty of about 2 dB in achieving error

free transmission. This can be attributed to roll-off in the frequency response of the modulators M_1 and M_2.

The subcarrier frequency f_{rf} can be readily scaled up with minimal power loss. Such higher frequency has benefits in terms of ability to carry more data.

The above-described embodiment of a fiber optic link transmission system could be readily extended to a systems utilizing multiple subcarrier channels. Referring now to Figure 23, each baseband information signal S_{i1}, S_{i2}, ... is applied to the IF port of a corresponding mixer $M^e_{0,1}$, $M^e_{0,2}$, ... and upconverted to the microwave frequency band by application of a corresponding microwave RF signal S_{rf1}, S_{rf2}, ... to the RF port of the corresponding mixer to produce a microwave modulated signal, i.e. baseband information signal S_{i1}, S_{i2}, ... modulated by microwave subcarrier signal S_{rf1}, S_{rf2}, ... The microwave modulated output signals of the mixers $M^e_{0,1}$, $M^e_{0,2}$, ... are applied by standard microwave transmission means, by wireless transmission in free space, or other means known in the art, to corresponding first optical modulators $M_{1,1}$, $M_{1,2}$, ... as corresponding modulated signals $S_{1,1}"$, $S_{1,2}"$, ... The first optical modulators $M_{1,1}$, $M_{1,2}$, ..., responsive to corresponding modulated signals $S_{1,1}"$, $S_{1,2}"$, ..., produce corresponding first modulated optical signals $L_{m1,1}$, $L_{m1,2}$, ... which are applied, preferably by polarization-maintaining optical fiber, to an

optical combiner 380. The optical combiner 380, preferably having low cross-interference, responsive to the first modulated optical signals $L_{m1,1}$, $L_{m1,2}$, ..., produces a combined first modulated optical signal L_{m1}'. This combined first modulated optical signal L_{m1}' includes the baseband information of baseband information signals S_{i1}, S_{i2}, ... multiplexed on separate subcarrier subchannels determined by the subcarrier signals S_{rf1}, S_{rf2}, ...

The combined first modulated optical signal L_{m1}' is transmitted, preferably by polarization-maintaining optical fiber, to a splitter 390, which produces received first modulated optical signals $L''_{m1,1}$, $L''_{m1,2}$, ..., and transmits them to corresponding second optical modulators $M_{2,1}$, $M_{2,2}$, ... Each second optical modulator $M_{2,1}$, $M_{2,2}$, ... selects a subchannel by application of a corresponding LO microwave signal $S''_{2,1}$, $S''_{2,2}$, ... to produce a corresponding second optical modulated signal $L_{m2,1}$, $L_{m2,2}$, ... Some or all of the second optical modulated signals $L_{m2,1}$, $L_{m2,2}$, ... are detected by a corresponding photoreceiver 260_1, 260_2, ... and processed to recover the data on the selected subchannel.

Alternatively, the receiver end of the system 290 (Figure 21), rather than the receiver end 400, could be utilized, with the microwave LO signal S''_2 tuned to select the desired channel.

Referring now to Figures 21 and 23, in an alternative configuration for the input end of a fiber optic link transmission system utilizing multiple subchannels, microwave modulated output signals of the mixers $M^e_{o,1}$, $M^e_{o,2}$, ... are combined by a microwave combiner (not shown) of sufficient bandwidth, the output of which is applied as signal S_i" to the first optical modulator M_1. The first modulated optical signal L_{m1} now includes the baseband information of baseband information signals S_{i1}, S_{i2}, ... multiplexed on separate subcarrier subchannels determined by the subcarrier signals S_{rf1}, S_{rf2}, ..., just as the combined first modulated optical signal L_{m1}' does. The first modulated optical signal L_{m1} can be processed as the combined first modulated optical signal L_{m1}' described above is to recover the data on a selected subchannel.

Referring now to Figure 24, in an optical fiber link transmission system 410, an optical modulator M_0 can be used to modulate the baseband information signal S_i. The optical modulator M_0 is preferably of the same type as optical interferometric modulators M_1 and M_2 described above.

The baseband information signal S_i is applied to the optical modulator M_0 which, responsive to source light L_i and the baseband signal S_i produces a modulated optical signal L_{m0}. This signal L_{m0} includes the source light L_i modulated by the baseband signal S_i. The modulated optical signal L_{m0} is applied to the

first optical modulator M_1. The first optical modulator M_1, responsive to the modulated optical signal L_{m0} and the subcarrier signal S_{rf} produces the first modulated optical signal L_{m1}. The first modulated optical signal L_{m1} is a subcarrier multiplexed signal and is further processed as in device 290 (Figure 21).

The fiber optic transmission system 410 utilizes a broadband modulator M_0 having a much wider bandwidth than an electrical mixer M_o^e of system 290. Therefore, this system 410 is capable of processing baseband information signals S_i with high information content and high bit rate.

Referring now to Figure 25, a fiber optic link transmission system utilizing multiple subcarrier channels has an optical interferometric modulator $M_{0,1}$, $M_{0,2}$, ... for each channel. Each baseband information signal S_{i1}, S_{i2}, ... is applied to the corresponding optical modulator $M_{0,1}$, $M_{0,2}$, ... which, responsive to it and to source light L_i, produces a corresponding modulated optical signal $L_{m0,1}$, $L_{m0,2}$, ... Each modulated optical signal $L_{m0,1}$, $L_{m0,2}$, ... includes the source light L_i modulated by the corresponding baseband signal S_{i1}, S_{i2}, ... Each modulated optical signal $L_{m0,1}$, $L_{m0,2}$, ... is applied to a corresponding first optical interferometric modulator $M_{1,1}$, $M_{1,2}$, ... Each first optical interferometric modulator $M_{1,1}$, $M_{1,2}$, ... responsive to the corresponding modulated optical signal $L_{m0,1}$, $L_{m0,2}$, ... and to a corresponding subcarrier signal S_{rf1}, S_{rf2}, ... produces a first

modulated optical signal $L_{m1,1}$, $L_{m1,2}$, ... Each first modulated optical signal $L_{m1,1}$, $L_{m1,2}$, ... is a subcarrier multiplexed signal and is further processed as described above and shown in Figure 23.

The foregoing descriptions of the preferred embodiments are intended to be illustrative and not limiting. Numerous modifications and variations can be made without departing from the spirit or scope of the present invention, The invention may be practiced otherwise than as specifically described.

ABSTRACT

A transmission system responsive to an electrical input information signal includes means for modulating the input signal with a microwave subcarrier signal to produce a subcarrier modulated signal. A first interferometric modulator responsive to a source light and to the subcarrier modulated signal produces a first modulated optical signal. A second interferometric modulator cascade coupled to the first modulator and being responsive to the first modulated optical signal and to a microwave local oscillator signal produces a second modulated optical signal. Means coupled between the first and second modulators transmit the first modulated optical signal from the first modulator to the second modulator. Means responsive to the second modulated optical signal produce an output signal.

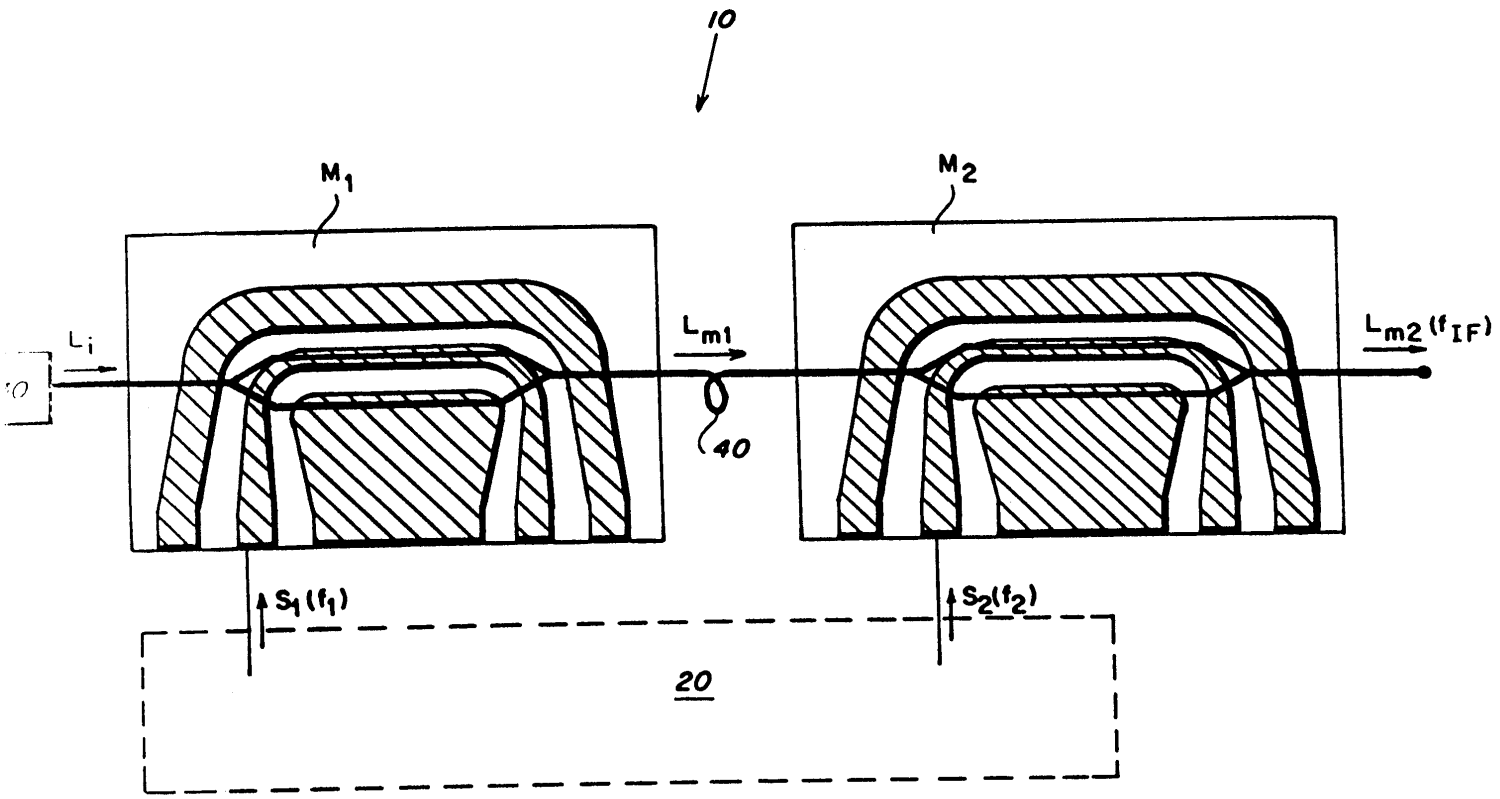

FIG. 1

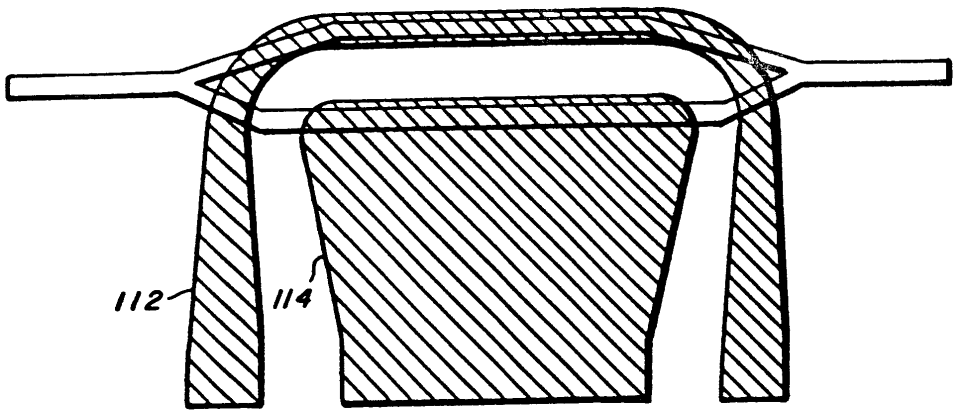

FIG. 2A

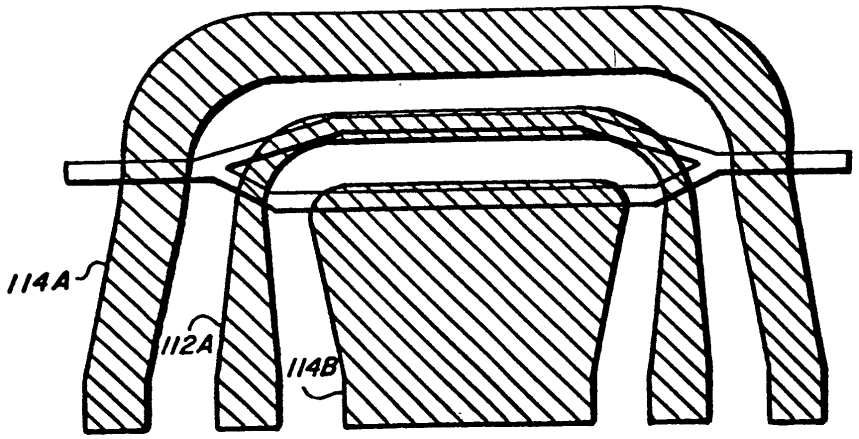

FIG. 2B

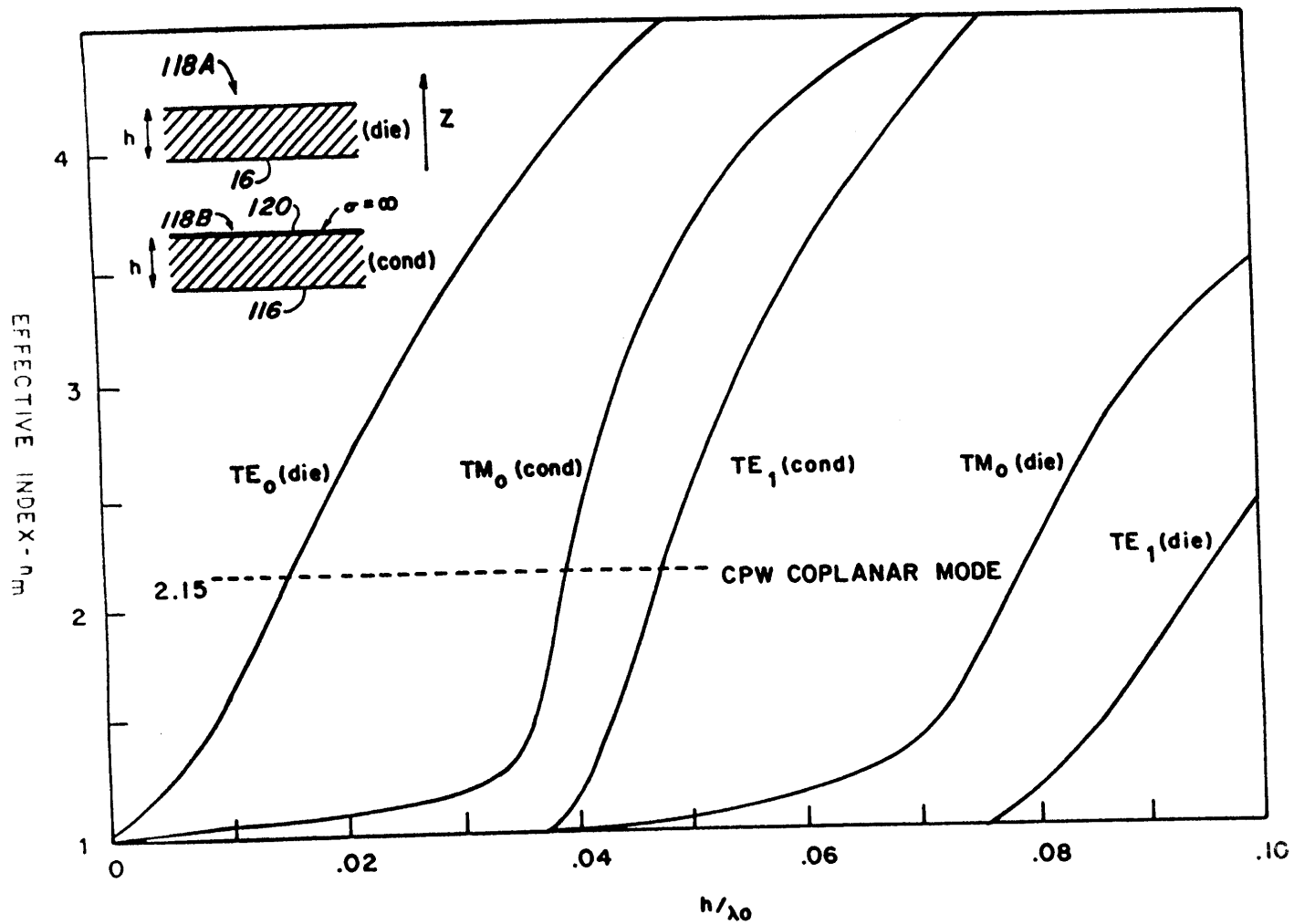
118A
h
(die)
Z
16
118B
120
σ = ∞
h
(cond)
116
EFFECTIVE INDEX - n_m
4
3
2
1
TE_0(die)
TM_0 (cond)
TE_1(cond)
TM_0 (die)
TE_1(die)
2.15
CPW COPLANAR MODE
0
.02
.04
.06
.08
.10
h/λ_0

FIG. 3

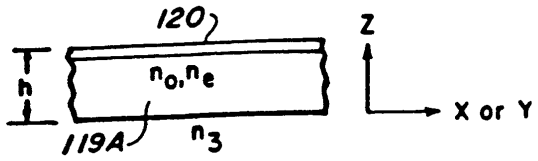

FIG. 3A

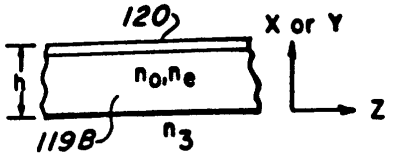

FIG. 3B

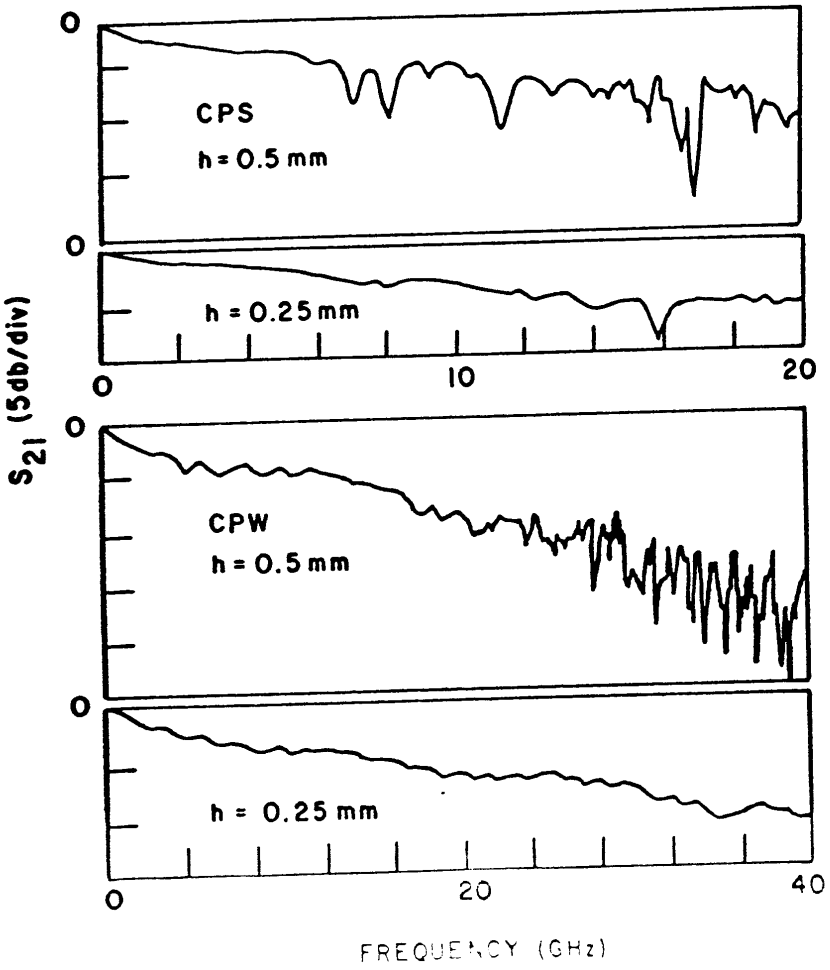

FIG. 4A

FIG. 4B

FIG. 4C

FIG. 4D

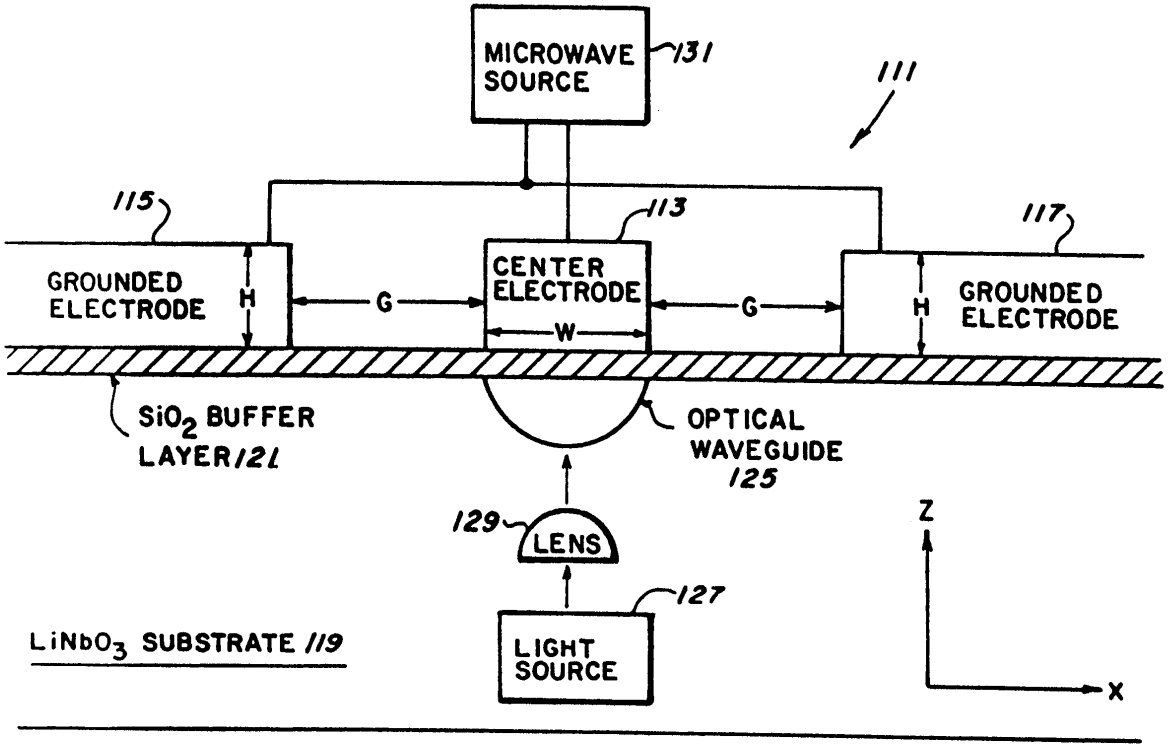
MICROWAVE SOURCE
131
111
115
113
117
GROUNDED ELECTRODE
H
G
CENTER ELECTRODE
W
G
H
GROUNDED ELECTRODE
SiO2 BUFFER LAYER 121
OPTICAL WAVEGUIDE 125
129
LENS
127
LiNbO3 SUBSTRATE 119
LIGHT SOURCE
Z
X

FIG. 5

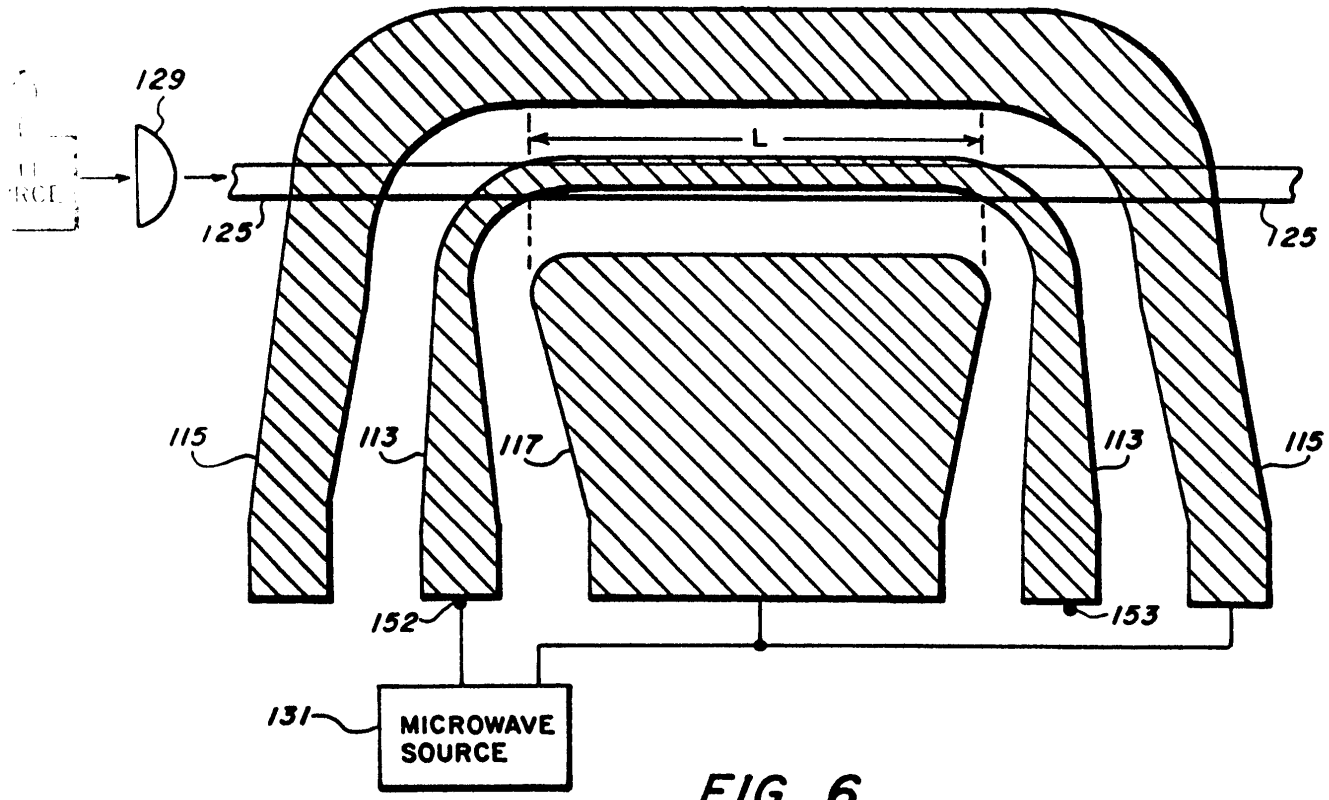

FIG. 6

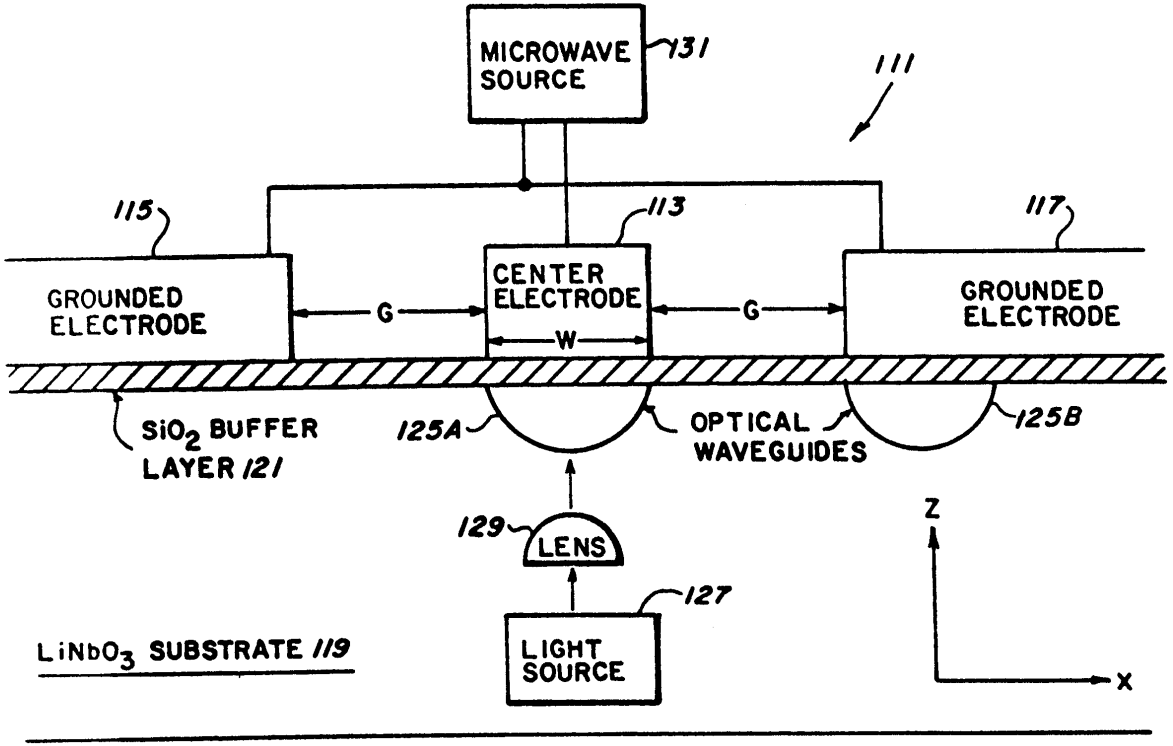
MICROWAVE SOURCE
131
111
115
113
117
GROUNDED ELECTRODE
G
CENTER ELECTRODE
W
G
GROUNDED ELECTRODE
SiO2 BUFFER LAYER 121
125A
OPTICAL WAVEGUIDES
125B
129
LENS
127
LIGHT SOURCE
LiNbO3 SUBSTRATE 119
Z
X

FIG. 7

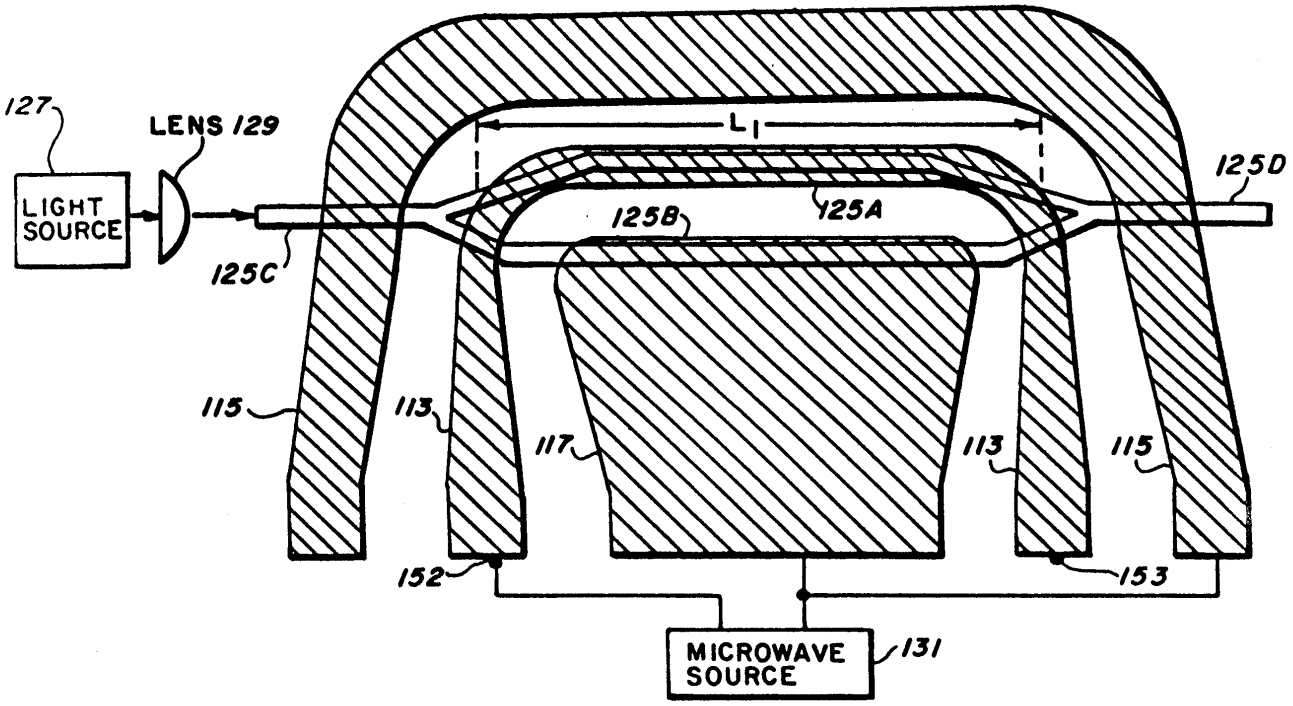
127
LENS 129
LIGHT SOURCE
125C
L1
125D
125B
125A
115
113
117
113
115
152
153
MICROWAVE SOURCE
131

FIG. 8

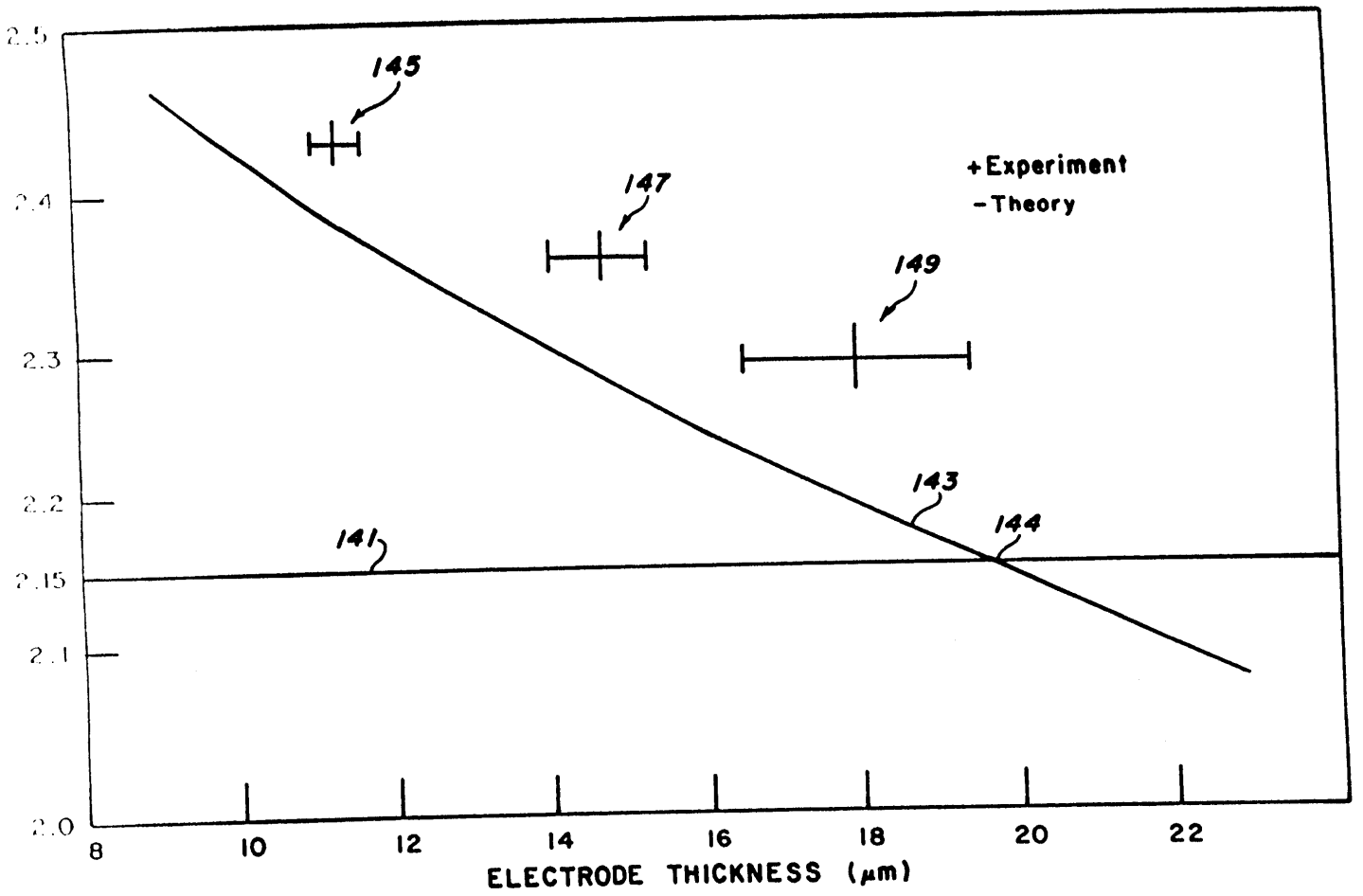
2.5
2.4
2.3
2.2
2.15
2.1
2.0
145
147
149
141
143
144
+Experiment
-Theory
8
10
12
14
16
18
20
22
ELECTRODE THICKNESS (μm)

FIG. 9

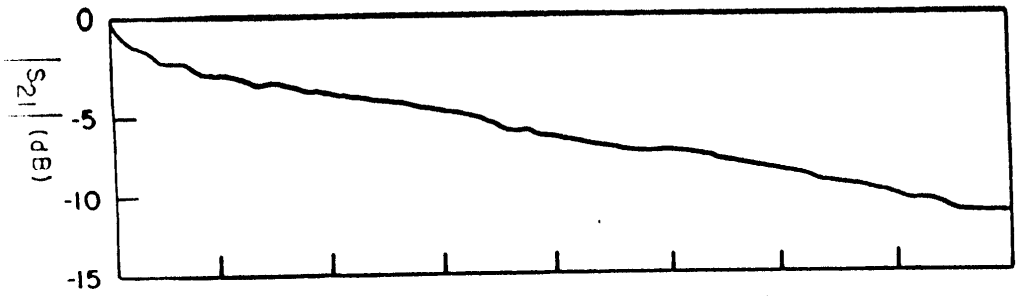

FIG. 10A

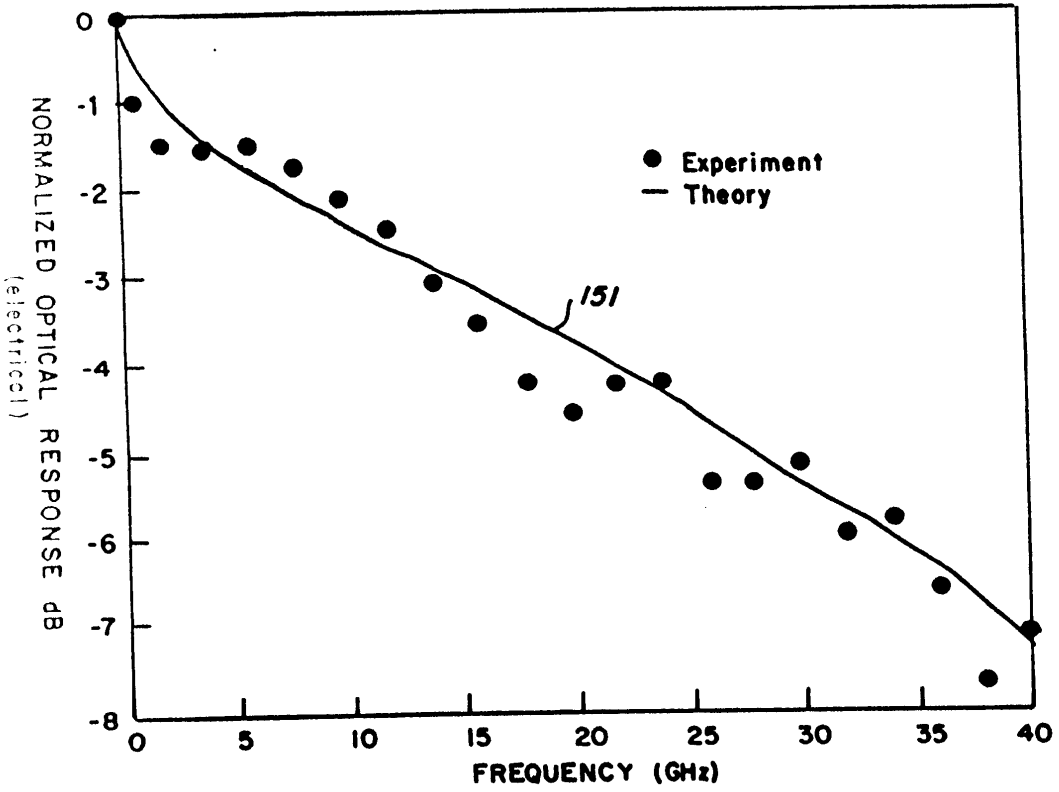

FIG. 10B

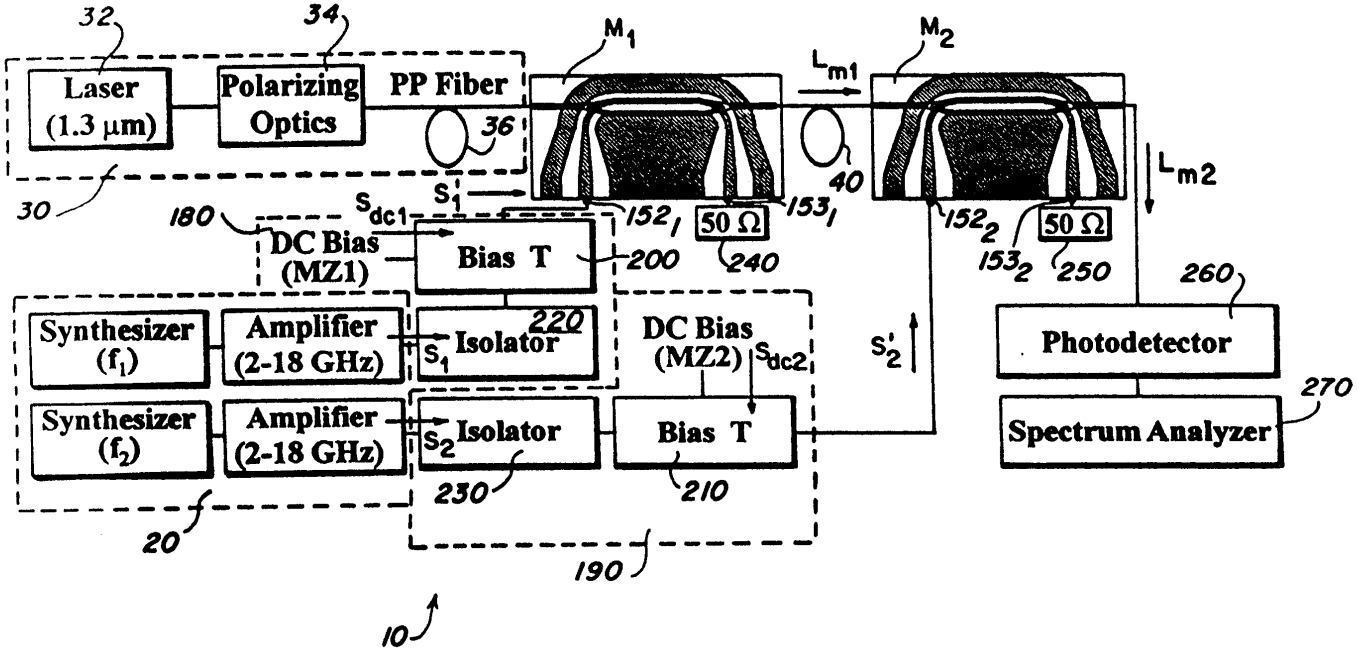
32
34
Laser
(1.3 μm)
Polarizing
Optics
PP Fiber
36
30
M1
M2
Lm1
Lm2
40
S1
Sdc1
180
DC Bias
(MZ1)
Bias T
200
152 1
153 1
50 Ω
240
152 2
153 2
50 Ω
250
260
Photodetector
270
Spectrum Analyzer
Synthesizer
(f1)
Amplifier
(2-18 GHz)
220
Isolator
S1
DC Bias
(MZ2)
Sdc2
S'2
Synthesizer
(f2)
Amplifier
(2-18 GHz)
S2
Isolator
230
Bias T
210
20
190
10

FIG. 11

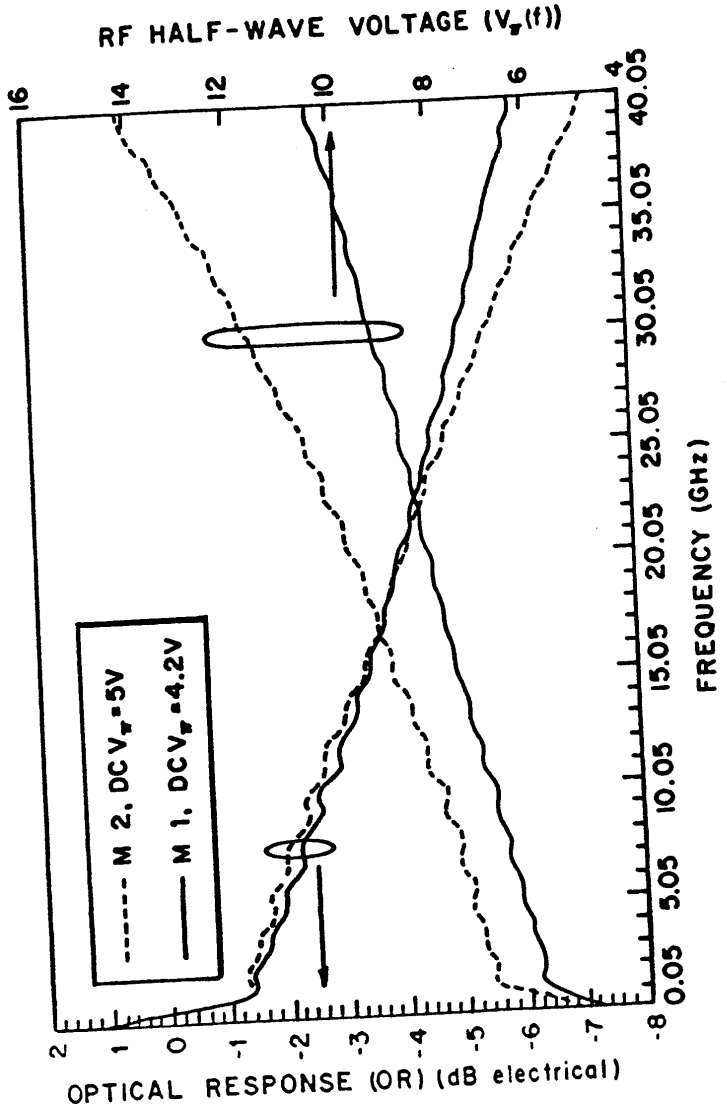
RF HALF-WAVE VOLTAGE ($V_\pi(f)$)
16
14
12
10
8
6
4
40.05
35.05
30.05
25.05
20.05
15.05
10.05
5.05
0.05
FREQUENCY (GHz)
M 2, DC V_π=5V
M 1, DC V_π=4.2V
2
1
0
-1
-2
-3
-4
-5
-6
-7
-8
OPTICAL RESPONSE (OR) (dB electrical)

FIG. 12

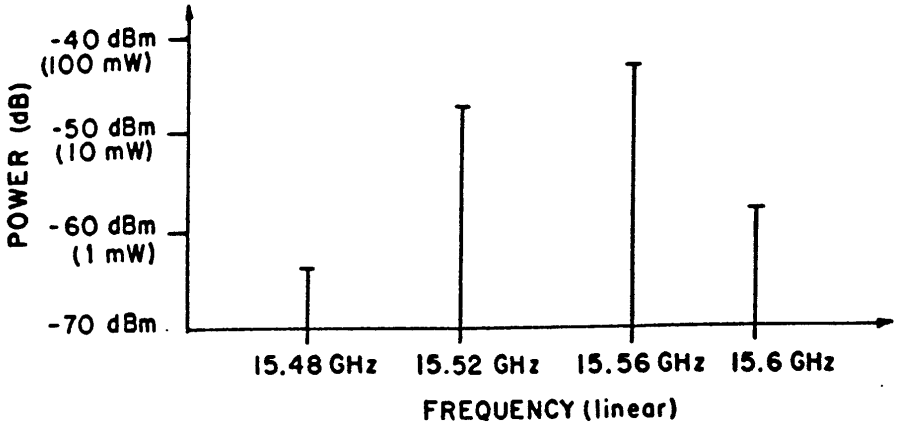
-40 dBm
(100 mW)
-50 dBm
(10 mW)
-60 dBm
(1 mW)
-70 dBm
POWER (dB)
15.48 GHz
15.52 GHz
15.56 GHz
15.6 GHz
FREQUENCY (linear)

FIG. 13

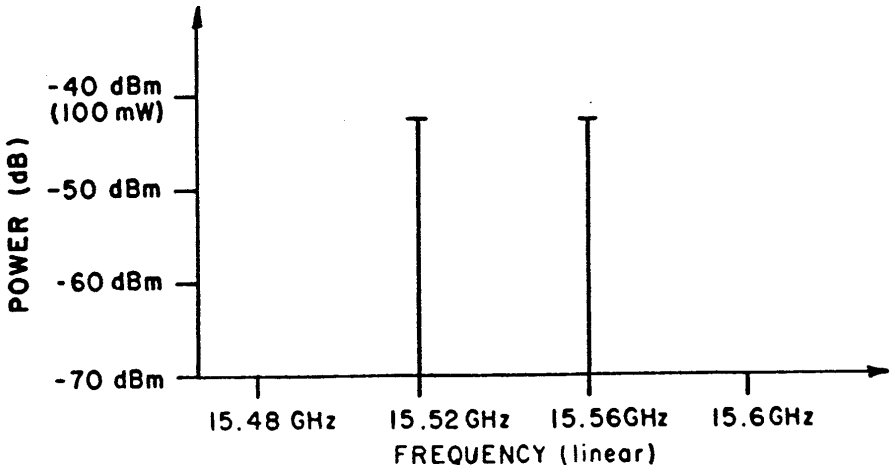
-40 dBm
(100 mW)
-50 dBm
-60 dBm
-70 dBm
POWER (dB)
15.48 GHz
15.52 GHz
15.56GHz
15.6GHz
FREQUENCY (linear)

FIG. 14

FIG. 15

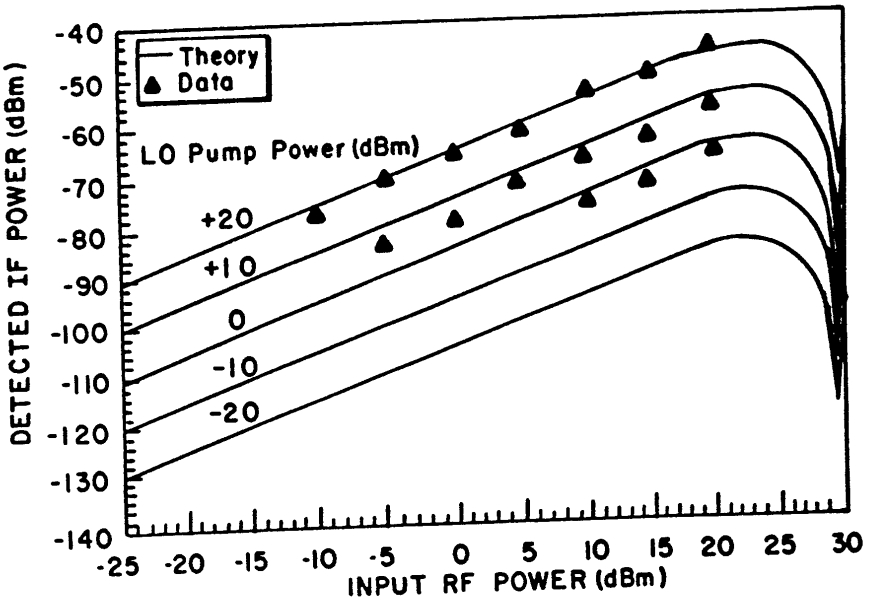
Theory
Data
LO Pump Power (dBm)
+20
+10
0
-10
-20
DETECTED IF POWER (dBm)
-40
-50
-60
-70
-80
-90
-100
-110
-120
-130
-140
-25 -20 -15 -10 -5 0 5 10 15 20 25 30
INPUT RF POWER (dBm)

FIG. 16

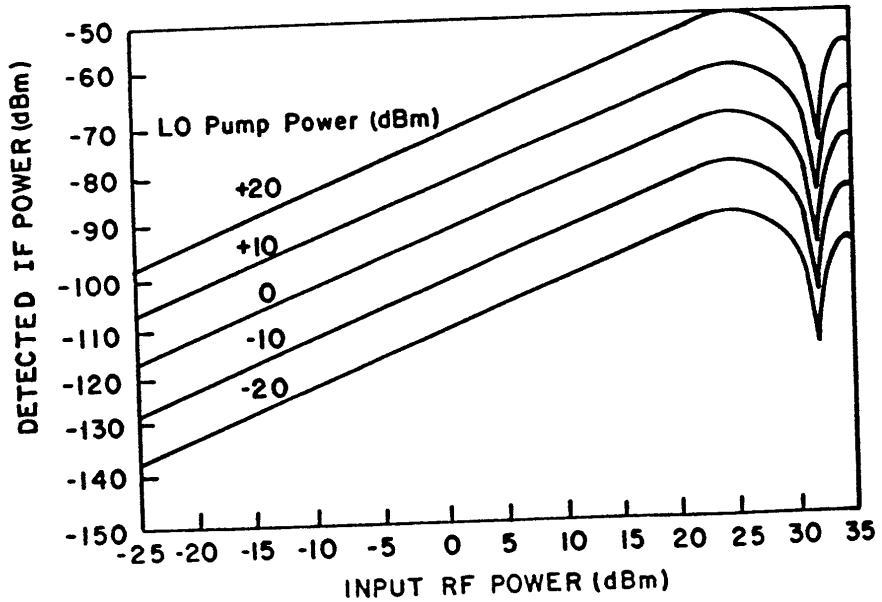
LO Pump Power (dBm)
+20
+10
0
-10
-20
DETECTED IF POWER (dBm)
-50
-60
-70
-80
-90
-100
-110
-120
-130
-140
-150
-25 -20 -15 -10 -5 0 5 10 15 20 25 30 35
INPUT RF POWER (dBm)

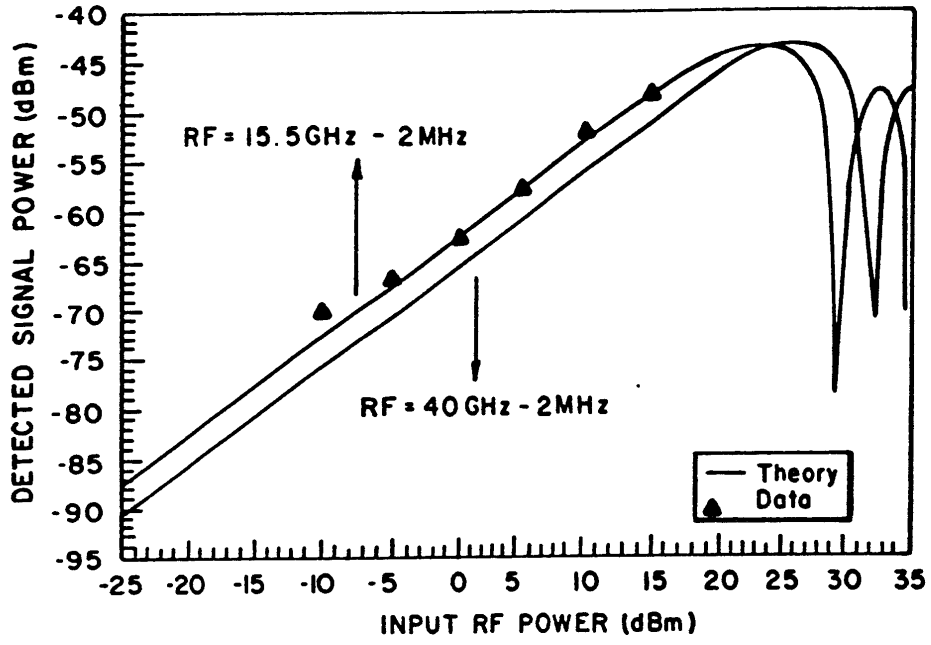
DETECTED SIGNAL POWER (dBm)
-40
-45
-50
-55
-60
-65
-70
-75
-80
-85
-90
-95
RF = 15.5GHz - 2MHz
RF = 40GHz - 2MHz
Theory
Data
-25 -20 -15 -10 -5 0 5 10 15 20 25 30 35
INPUT RF POWER (dBm)

FIG. 17

FIG. 18

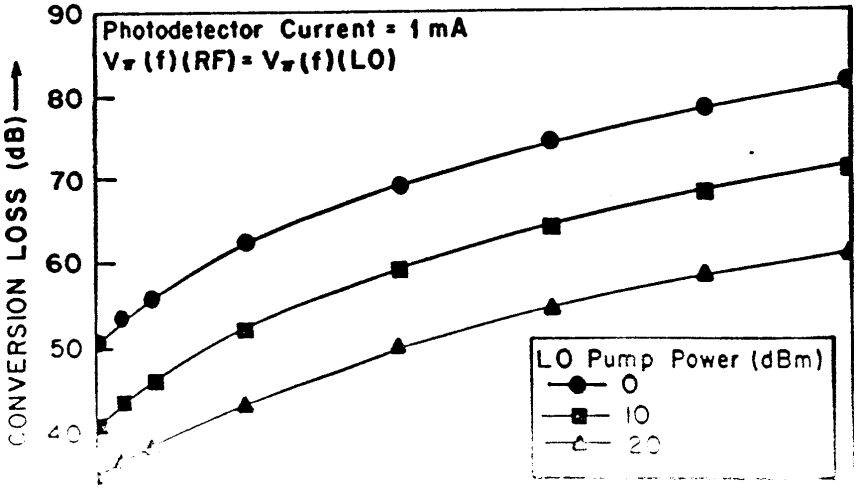
Photodetector Current = 1 mA
$V_{IF}(f)(RF) = V_{IF}(f)(LO)$
CONVERSION LOSS (dB)
90
80
70
60
50
40
LO Pump Power (dBm)
0
10
20

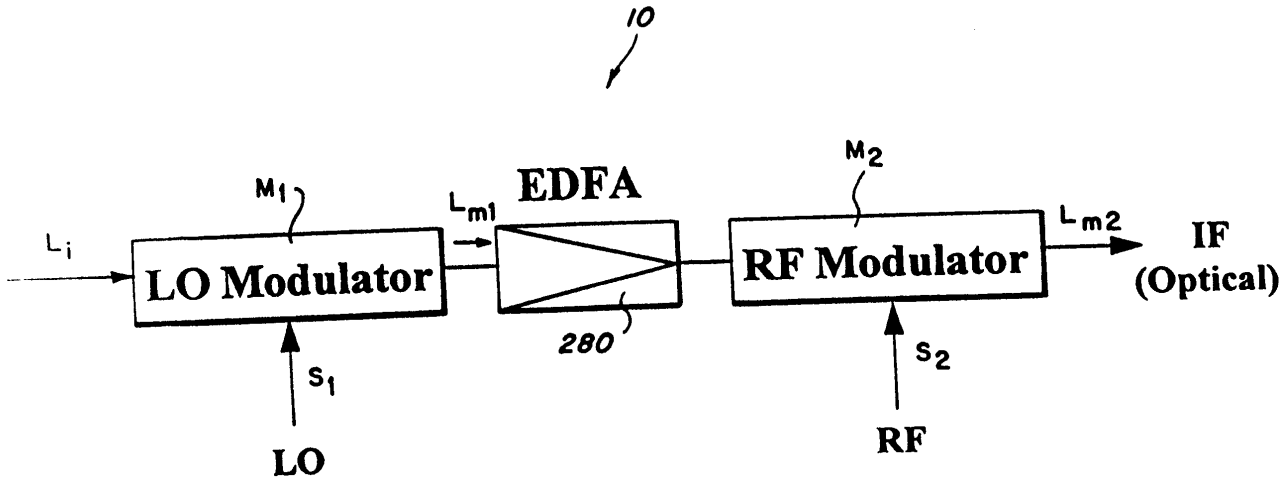
10
M1
EDFA
M2
Li
LO Modulator
Lm1
Lm2
IF
(Optical)
RF Modulator
280
S1
S2
LO
RF

FIG. 19

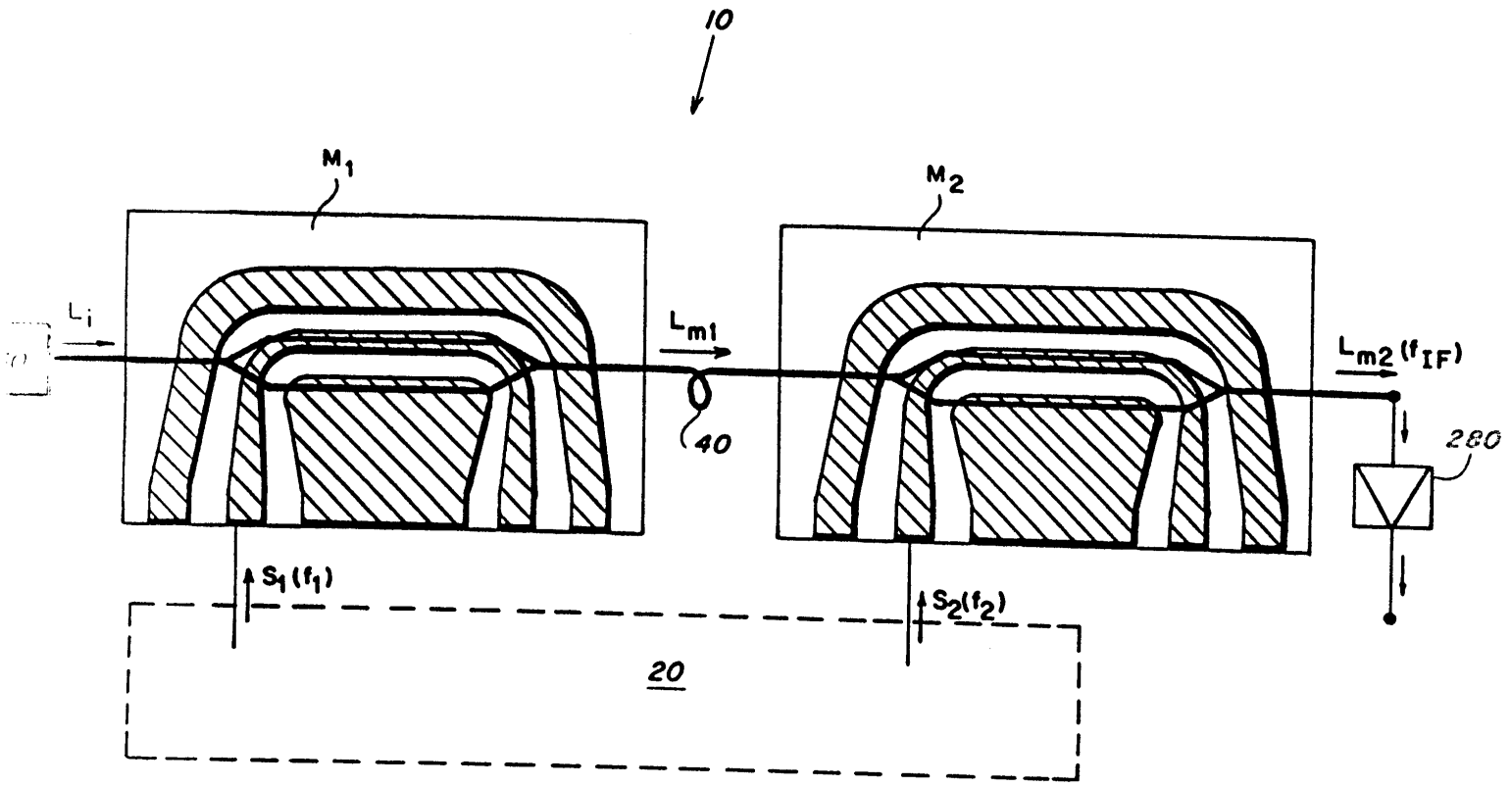

FIG. 20

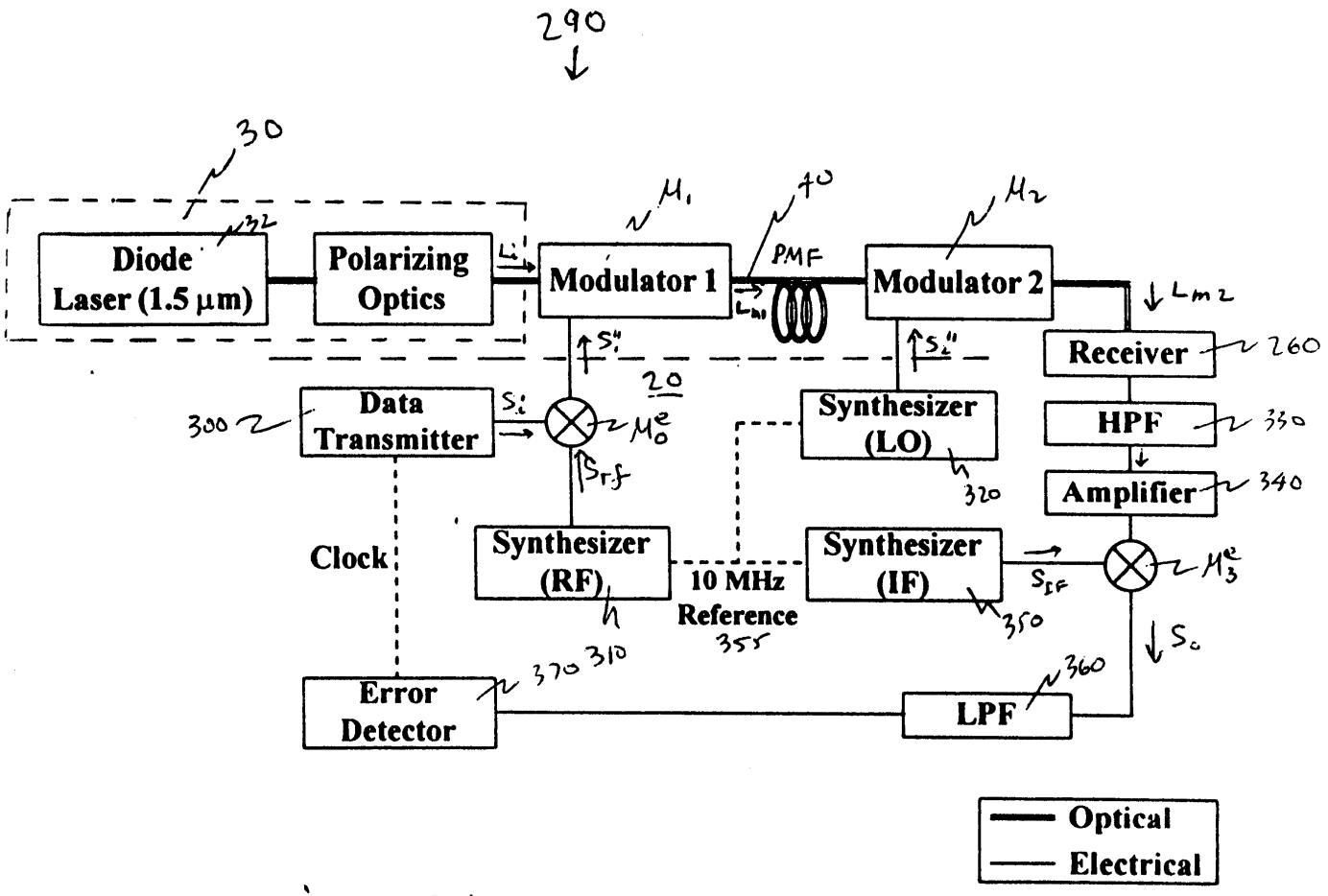

Figure 21

FIG 1

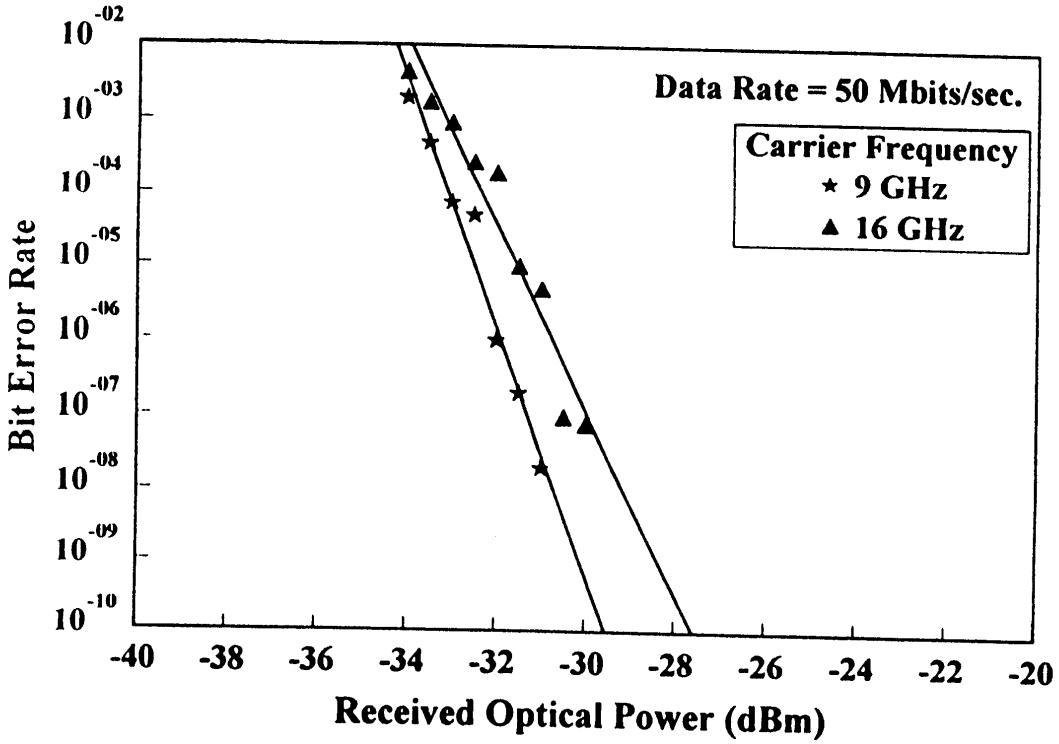
Data Rate = 50 Mbits/sec.
Carrier Frequency
★ 9 GHz
▲ 16 GHz
Bit Error Rate
10^-02
10^-03
10^-04
10^-05
10^-06
10^-07
10^-08
10^-09
10^-10
-40 -38 -36 -34 -32 -30 -28 -26 -24 -22 -20
Received Optical Power (dBm)

Figure 22

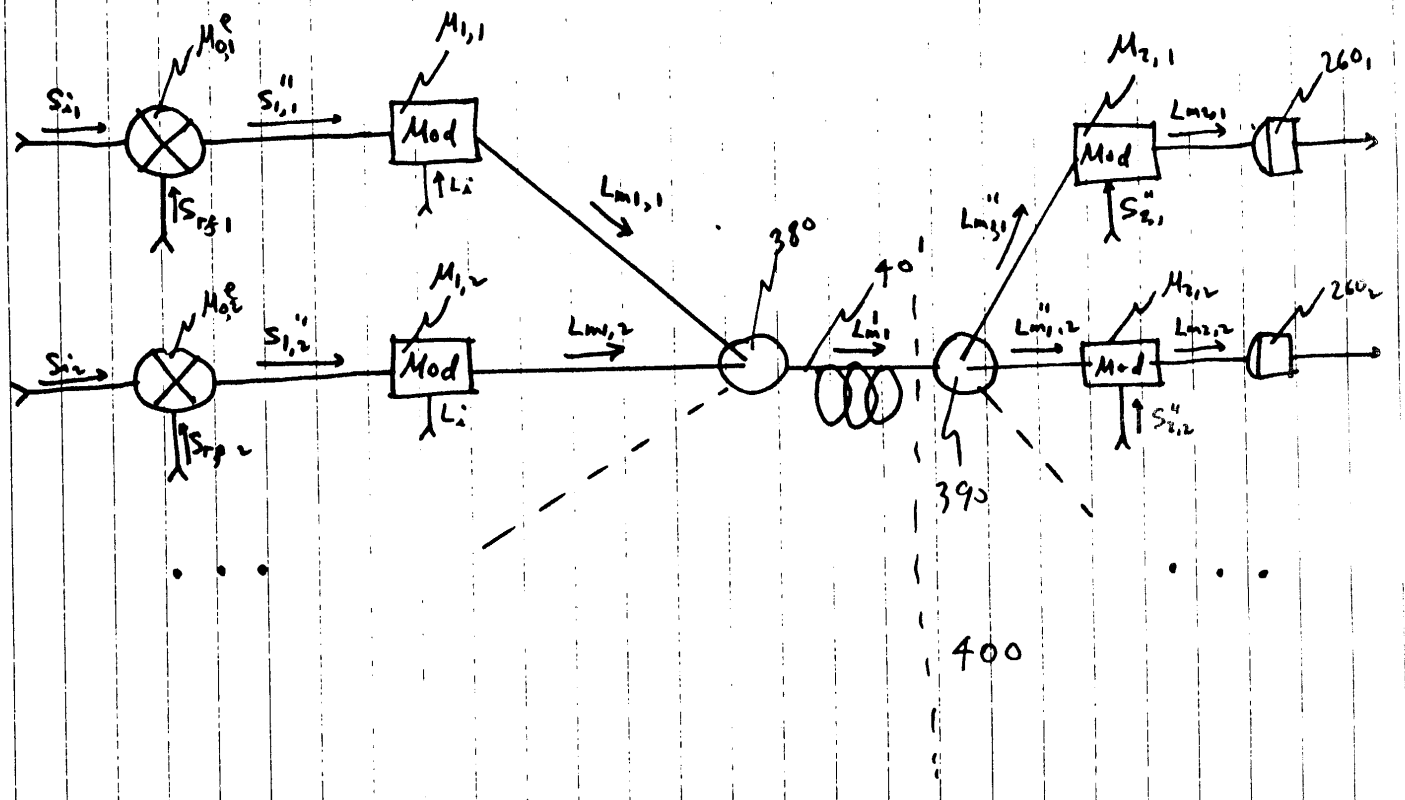

Figure 23

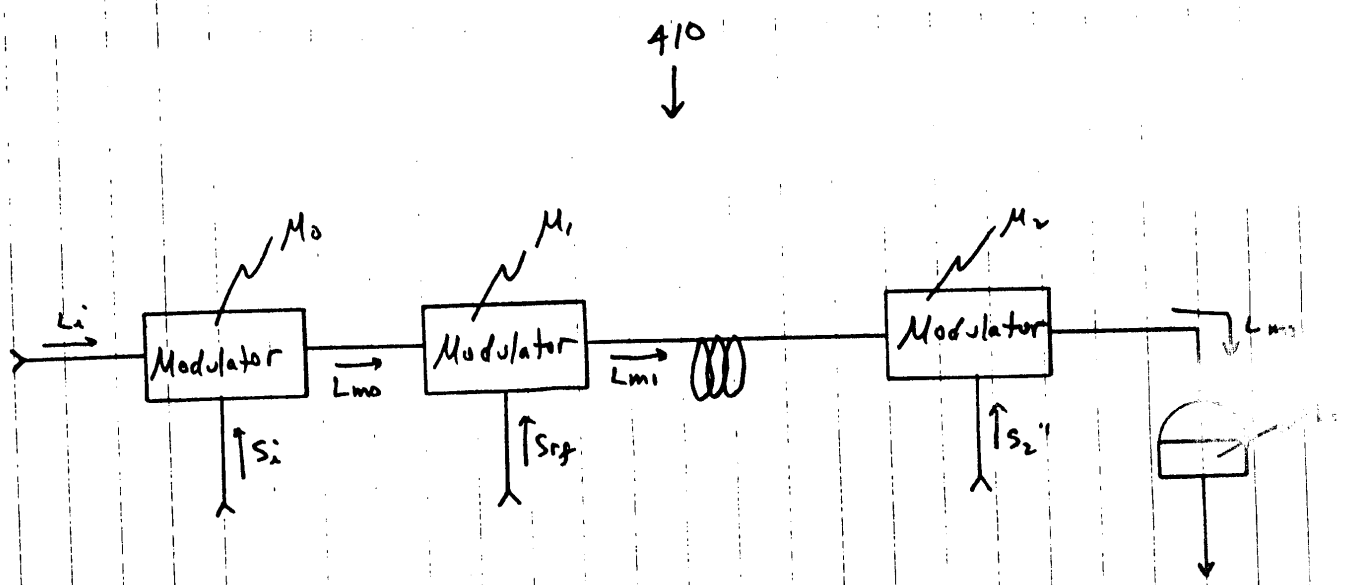
410
M_0
M_1
M_2
L_i
Modulator
Modulator
Modulator
L_{mo}
L_{m1}
L_{m2}
S_i
S_{rf}
S_2

Figure 24

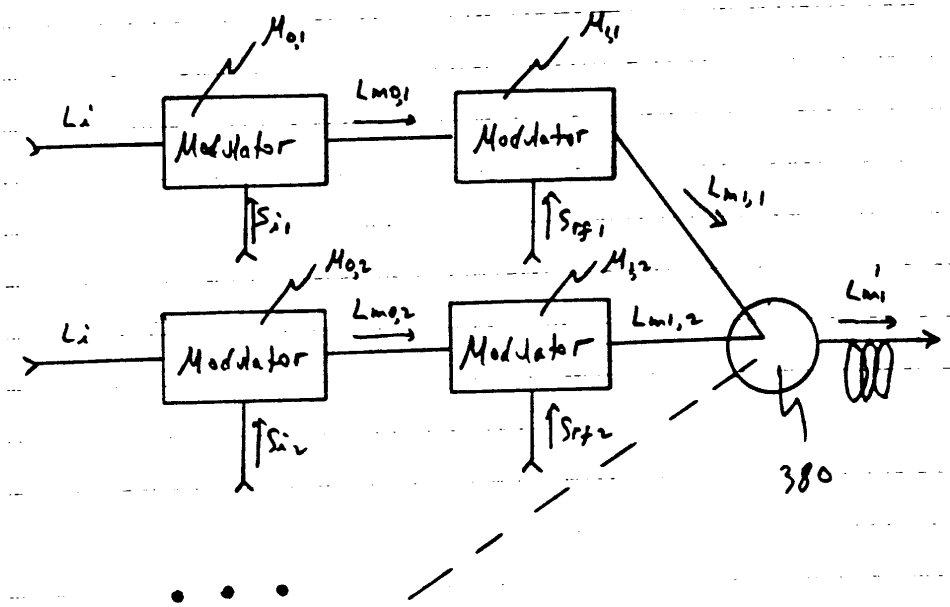

Figure 25